1,4-Dioxane Induces Epithelial-Mesenchymal Transition and Carcinogenesis in an Nrf2-Dependent Manner

Ziwei Wang[1] | Chitra Thakur[1] | Zhuoyue Bi[1] | Yiran Qiu[1] | Wenxuan Zhang[1] | Haoyan Ji[1] | Arjun K. Venkatesan[2,3] | Sashank Cherukuri[1] | Ke Jian Liu[1] | John D. Haley[1] | Xinwei Mao[4,5] | Jaymie Meliker[6] | Fei Chen[1]

[1]Stony Brook Cancer Center, Department of Pathology, Renaissance School of Medicine, Stony Brook University, Stony Brook, New York, USA | [2]Civil Engineering, School of Marine and Atmospheric Sciences, Stony Brook University, Stony Brook, New York, USA | [3]Department of Civil and Environmental Engineering, New Jersey Institute of Technology, Newark, New Jersey, USA | [4]Department of Civil Engineering, College of Engineering and Applied Sciences, Stony Brook University, Stony Brook, New York, USA | [5]New York State Center for Clean Water Technology, Stony Brook University, Stony Brook, New York, USA | [6]Department of Family, Population and Preventive Medicine, Renaissance School of Medicine, Stony Brook University, Stony Brook, New York, USA

Correspondence: Ziwei Wang (Ziwei.Wang@stonybrook.edu) | Fei Chen (Fei.Chen.1@stonybrook.edu)

ABSTRACT

The carcinogenic potential of the environmental pollutant 1,4-dioxane (1,4-D) in humans is not yet fully understood or recognised. In this study, we provide evidence that 1,4-D acts as a carcinogen in human epithelial cells. Using the human bronchial epithelial cell line BEAS-2B, with or without CRISPR-Cas9-mediated Nrf2 knockout, we demonstrate that continuous exposure to environmentally relevant concentrations of 1.25–20 ppm 1,4-D over 2 months induces malignant transformation in an Nrf2-dependent manner. Transformed cells exhibit enhanced anchorage-independent growth in soft agar, increased migration and invasion, and tumorigenic potential in a xenograft mouse model. Integrated RNA sequencing and proteomics analyses reveal that 1,4-D robustly activates Nrf2 signalling, driving extracellular vesicle (EV) biogenesis and cargo loading with syndecan 4 (SDC4) and other proteins, including COL12A1, CAPG and NNMT, which are associated with epithelial-mesenchymal transition (EMT) and cancer metastasis. Nrf2 knockout reduces SDC4 expression and its incorporation into EVs, leading to decreased EV uptake by recipient cells. Unlike EVs from 1,4-D-transformed WT cells, which enhance the proliferation, migration and invasion of recipient cells, EVs from 1,4-D-transformed Nrf2 KO cells exhibit a diminished capacity to promote these EMT properties. Furthermore, we demonstrate that the Nrf2 target gene *SDC4*, induced by 1,4-D and enriched in EVs, plays a critical role in EV uptake by recipient cells, thereby facilitating EMT propagation. Collectively, our findings suggest that 1,4-D is a human carcinogen, with its carcinogenicity largely dependent on Nrf2 activation, which orchestrates the biogenesis of EVs with EMT-promoting functions.

1 | Introduction

1,4-Dioxane (1,4-D) is a heterocyclic organic compound of ether with oxygen atoms at positions 1 and 4 of dioxane, which is widely used in the manufacture of chlorinated solvents as a stabiliser. It is highly persistent in aquifer systems, making removal challenging. According to the Environmental Working Group (EWG)'s Tap Water database, over 7 million people across 27 states receive water from public systems where the average 1,4-D levels exceed the cancer risk thresholds of Environmental Protection Agency's

(EPA). Several hot spots of 1,4-D contamination in drinking water have been identified, including Long Island in New York, the Cape Fear River basin in North Carolina, and southeastern Los Angeles County, California (Godri Pollitt et al. 2019). In some cases, the concentration of 1,4-D in municipal supply wells and wastewater streams exceeds 200 to 2000 ppm (Zenker et al. 2003). However, the true extent of nationwide 1,4-D contamination may be underestimated due to incomplete data collection, especially concerning small or medium-sized water supply systems and private water wells. The latest ranking of drinking water chemical risks, based on population exposure, highlights 1,4-D among the top 25 of 139 analysed chemicals, surpassing widely studied contaminants such as Per- and Polyfluoroalkyl Substances (PFAS) and carcinogenic metals (Rosenblum et al. 2024). Recent assessments have found 1,4-D in certain cosmetic products, baby soaps, and baby diapers, with concentrations ranging from 10 to 80 ppm (Ginsberg et al. 2022; Lin et al. 2023). While the EPA considers 1,4-D as a probable human carcinogen based on toxicology studies in mice and rats and has established a guideline of 0.35 ppb for drinking water, the lack of sufficient data hinders the development of maximum contaminant levels (MCLs) or federal polices for risk assessment and mitigation of 1,4-D contamination.

Animal studies indicated that exposure to high doses of 1,4-D at 393–5738 ppm (66–964 mg/kg per day) resulted in increased activity of Cytochrome P450 family 2E1 (CYP2E1) enzymes, oxidative stress and hepatic genomic abnormality in mice (Godri Pollitt et al. 2019; Wang et al. 2022). Long-term exposure studies in mice and rats have shown that 1,4-D disrupts regenerative repair, promotes cell proliferation and may even lead to tumorigenesis (Lafranconi et al. 2023). Several types of malignancies were reported in animals exposed to 1,4-D, including hepatocellular adenomas (Dourson et al. 2014), nasal vestibule squamous cell carcinoma, lung cancer, skin cancer, mammary gland cancers, peritoneal mesotheliomas and gall-bladder tumours (Lafranconi et al. 2023; Sweeney et al. 2008). While 1,4-D itself may be not mutagenic in combined *in vitro* genotoxicity tests, *in vivo* genotoxicity is likely due to the presence of other environmental risk factors and underlying disease processes (Dourson et al. 2017; Gi et al. 2018; Ginsberg et al. 2022). Furthermore, compelling evidence suggests that 1,4-D induces oxidative stress in cells, causing DNA damage. A study in F344 *gpt* delta rats exposed to 1,4-D in drinking water has shown a dose-dependent increase in DNA adducts in the livers (Totsuka et al. 2020). However, there is a lack of direct evidence that 1,4-D is mutagenic and carcinogenic in humans at environmentally relevant levels. Due to its nonlinear toxicokinetic, understanding the mechanism involving in the genotoxicity and carcinogenicity of 1,4-D is challenging. Studies are urgently needed to further elucidate the carcinogenic potential of 1,4-D in humans.

NFE2 Like BZIP Transcription Factor 2 (Nrf2), an evolutionally conserved transcription factor that plays a crucial role in redox regulation (Hahn et al. 2015), has garnered attention as a key player in cancer progression, tumour cell metastasis and therapeutic resistance (Ni et al. 2014; Rojo de la Vega et al. 2018). Our pervious chromatin immunoprecipitation sequencing (ChIP-seq) data from arsenic carcinogenesis study showed the direct regulation of Nrf2 on the genes related to glycolysis and cancer cell stemness, such as *MYC*, *SOX2*, *KLF4*, *CD44*

and *EGFR*, particularly under stress conditions (Bi et al. 2020). Moreover, a recent study by Chen et al. (2022) revealed Nrf2 activation in mouse tissues following 5000 ppm of 1,4-D in drinking water. Additionally, emerging evidence underscores the pivotal roles of extracellular vesicles (EVs) in various stages of cancer development, particularly in cancer metastasis (Kalluri and McAndrews 2023). By packaging and transferring proteins, DNAs, RNAs, lipids and metabolites, EVs act as central mediators of intercellular communication within the tumour microenvironment, influencing tumour growth and dissemination. Some studies have also linked Nrf2-dependent EV biogenesis to antioxidant defence (Gao et al. 2021), anti-inflammation (Xu et al. 2022) and redox balance (Tian et al. 2022; Tian et al. 2021). While extensive research has focused on the carcinogenic effects of high-dose 1,4-D exposure in animal models, the potential carcinogenicity of environmentally relevant concentrations in human cells remains largely unexplored. Unravelling Nrf2's role in this process could provide critical insights into the mechanisms underlying 1,4-D-induced carcinogenesis and its broader implications in environmental health.

In this study, we demonstrate that the carcinogenic potential of 1,4-D is mediated through Nrf2 activation and Nrf2-dependent EV biogenesis, which ultimately promotes EMT and cancer metastasis. Using a combination of cell transformation assays, cell-derived xenograft models, transcriptomics and proteomics, we investigated the role of Nrf2 in 1,4-D-induced carcinogenesis and the impact of Nrf2-dependent EV biogenesis on EMT. Notably, the insights gained from this study could help in developing strategies to mitigate the adverse health effects of 1,4-D exposure and provide novel perspectives on how Nrf2-dependent EVs contribute to chemical carcinogenesis. A deeper understanding of these mechanisms may open new avenues for preventing and treating chemical-induced cancers.

2 | Materials and Methods

2.1 | Cell Culture

The human bronchial epithelial cell line BEAS-2B and the human non-small cell lung cancer derived hypotriploid alveolar basal epithelial cells A549, purchased from the American Type Culture Collection (ATCC, Manassas, VA), were maintained in complete medium at 37°C under 5% CO_2. The complete medium consisted of DMEM (Gibco, cat#11965092) with 5% fetal bovine serum (R&D systems, cat#S11150), 1% penicillin-streptomycin (Gibco, cat#15140122) and 1% L-Glutamine (Gibco, cat#25030081). The culture medium was changed every other day, and cell passage was performed every week.

2.2 | Generation of Nrf2 Depletion Stable Cell Lines

Nrf2 knockout was achieved using CRISPR-Cas9 gene editing as outlined by (Bi et al. 2020). Briefly, single guide RNAs (sgRNAs) targeting exon 2 of the human Nrf2 gene were designed with CRISPOR (http://crispor.tefor.net/). Two high-scoring sgRNAs were selected: sgRNA-1 (5′-TATTTGACTTCAGTCAGCGA-3′); sgRNA-2 (5′-GCGACGGAAAGAGTATGAGC-3′). Each

double-strand sgRNA was ligated into pSpCas9-2A-Blast vector (Addgene, cat#118055). BEAS-2B cells were infected with the constructed pSpCas9-2A-Nrf2 vector by Lipofectamine 2000 reagent (Invitrogen, cat#11668-018) according to the manufacturer's instructions. Following blasticidin selection at 4 μg/mL, approximately 20 colonies per sgRNA transfection were analysed by Western blotting to assess Nrf2 expression. Colonies lacking Nrf2 protein expression were classified as knockout (KO), while those with Nrf2 protein expression were classified as wild type (WT).

2.3 | 1,4-D Treatment

WT and Nrf2 KO cells were adapted through several generations of culture before 1,4-D treatment. The concentrations of 1,4-D (Sigma-Aldrich, cat#CRM48367) were chosen to reflect environmental contamination levels. Cells were exposed to 1,4-D at concentrations of 1.25, 2.5, 5.0, 10 and 20 ppm, while control cells were treated with an equivalent volume of vehicle solution, methanol. To develop 1,4-D-transformed cell models, both WT and Nrf2 KO cells underwent continuous treatment with 1,4-D at the specified concentrations for 2 months.

2.4 | Nucleus Extraction and Fractionation

After overnight incubation, cells were exposed to 1,4-D with concentrations of 1.25–20 ppm for 6 h. Nuclear extraction and fractionation were performed using the Nuclear Extraction Kit (Abcam, Cat#ab221978) in accordance with the manufacturer's guidelines. Protein expressions were evaluated via Western blotting, with Histone H3 and β-tubulin serving as nuclear and cytoplasmic markers, respectively.

2.5 | Nrf2 and AHR Luciferase Reporter Assay

To prepare the antioxidant response element (ARE, Nrf2-binding element) luciferase reporter construct, oligonucleotides (GTGACAAAGCACCCGTGACAAAGCACCCGTGACAAAG-CACCCGTGACAAAGCA) were ligated to the *ScaI* and *NheI* site of the PGL3-promoter vector (Addgene, cat#212939). Cells seeded in 24-well plate were co-transfected with 0.8 μg ARE luciferase reporter construct and 0.08 μg pRL-SV40P (Addgene, cat#27163) to express firefly luciferase under Nrf2 activation and renilla luciferase, respectively. Following treatment, cells were processed using Dual-Luciferase Reporter Assay System (Promega, cat#E1910) according to the manufacturer's protocol. Both luciferase activities were sequentially measured using a VARIOSKAN LUX (Thermo Scientific). AHR activation was assessed by the Human AHR luciferase Reporter Assay Kit (INDIGO Biosciences, cat#IB06001) following the manufacturer's instructions.

2.6 | Malignant Transformation of the Cells

The status of malignant transformation of the cells was monitored by surrogate markers including cell proliferation assay, anchorage-independent growth (colony formation) assay in soft agar, plate clonogenic growth, migration and invasion. For cell proliferation assay, 5×10^3 cells were seeded in the 96-well plates for 24 h, and then incubated with MTT (Sigma-Aldrich, cat#M2003) at a final concentration of 0.5 mg/mL for 4 h. The absorbance is analysed spectrophotometrically at 570 nm. For colony formation assay in soft agar, 5×10^3 cells/well were embedded in DMEM containing 0.3% agar (BD Microbiology, cat#214010), and then inoculated on 0.5% agar (diluted by 2×DMEM) in a 6-well plate for two weeks. Colonies stained with 1.0 mg/mL MTT were viewed under a microscope for counting. For plate clonogenic growth, 5×10^2 cells/well were seeded in the 6-well plate and cultured for 2 weeks. Colonies stained with 0.125% crystal violet were counted and imaged under a microscope. Cell number in each colony was calculated by using ImageJ v 1.53m (https://ij.imjoy.io/).

For cell migration and invasion assays, 2.5×10^4 cells/well resuspended in 100 μL serum-free culture medium were seeded into the upper chamber of 24-well Transwell (Corning, cat#CLS3464), and 600 μL of culture medium containing 10% FBS was added to the lower chamber. After 24-h incubation, cells in the upper chamber were fixed with 4% paraformaldehyde and stained with 0.125% crystal violet. Cells on the upper surface of the chamber were gently wiped away with a cotton swab. Photographs were taken using an inverted microscope, and cells were counted using ImageJ software. The protocol of invasion assay is the same as migration assay, but the difference is that Transwell used in invasion assay needs to be pre-coated with Matrigel Matrix (Corning, cat#CLS356234) in DMEM (1:7 ratio).

2.7 | Mouse Xenograft Experiment

Four-week-old female NOD scid gamma (NSG) mice were purchased from the Jackson Laboratory (Boston, MA), and maintained in compliance with federal guidelines. All animal use and experimental procedures were approved by the Institutional Animal Care and Use Committee (IACUC) at Stony Brook University (2021-00104). Mice were randomly divided into four groups ($n = 5$): WT, WT with 1,4-D treatment, Nrf2 KO, Nrf2 KO with 1,4-D treatment. After an adaptation period, each mouse received a subcutaneous injection of 2×10^6 cells. Tumour volumes were measured after 4 weeks. Mice were euthanised when the diameter of a subcutaneous tumour reaching 2 cm or no subcutaneous tumour was observed within 120 days post-injection. Tumour tissues were fixed with 10% formalin and processed with Haematoxylin and Eosin (H&E) staining.

2.8 | Western Blotting

Cells were lysed in ice-cold RIPA buffer containing 1 mM of phenylmethanesulfonyl fluoride (PMSF) (Sigma-Aldrich, cat#P7626). Total proteins were extracted according to the method previously described (Bi et al. 2020) and quantified by Pierce BCA Protein Assay Kit (Thermo Scientific, cat#23225). A total of 30 μg total proteins were separated by 10% SDS-PAGE and were transferred to a polyvinylidene fluoride (PVDF) membrane (Thermo Fisher, cat#YJ382392). The membranes were blocked by 5% fat-free milk and then incubated with primary antibodies and secondary antibodies as detailed in Table S1. Immunolabelling

was visualised using the ChemiDoc MP imaging system (Bio-Rad). Densitometry analysis was conducted using ImageJ software.

2.9 | Quantitative Real-Time PCR (qRT-PCR)

Total RNA was extracted using TRIzol (Invitrogen, cat#15596018). Reverse transcription and qRT-PCR were carried out with the high-capacity cDNA Reverse Transcription Kit (Thermo Fisher, cat#2616251) and SYBR Green PCR Master Mix (Thermo Fisher, cat#2211538), respectively. GAPDH was used as an internal control for the $2^{-\Delta\Delta Ct}$ method to determine the relative expression of mRNAs. The primers used for qRT-PCR are listed in Table S2.

2.10 | RNA-Sequencing (RNA-Seq) Analysis

Cells were collected for RNA extraction, followed by library preparation and RNA-seq using the Illumina NovaSeq6000 system. The filtered raw data was mapped to the reference genome *Homo sapiens* (GRCh38/hg38). Gene expression levels were estimated based on normalised FPKMs (Fragments per Kilobase Million). Differences in gene expression between groups were identified through pairwise comparison. Genes with a fold-change greater than 1.2 and *p* value less than 0.05 were regarded as differentially expressed genes (DEGs). Biological annotation of the DEGs was performed using gene ontology (GO) pathway analysis and gene set enrichment analysis (GSEA) via R software with clusterProfiler v.4.12.0 package (Wu et al. 2021). Significance was defined as *p* value < 0.05.

2.11 | EV Isolation and Characterisation

EVs were isolated from cell culture supernatants. Cells were plated at a density of 5×10^5 per 15 cm dish and cultured in EV-free medium (complete medium depleted of FBS-derived EVs by centrifugation at $100,000 \times g$ for 18 h) for 7 days. The culture media from 20 plates were polled and subjected to sequential centrifugation steps at $300 \times g$ for 10 min, $2000 \times g$ for 30 min, $10,000 \times g$ for 45 min to remove cells, cell debris and microvesicles. Subsequently, the supernatants were filtered through a 0.45 µm membrane, and then centrifuged twice at $100,000 \times g$ for 70 min. The size distribution and concentrations of EVs were measured using a nanoparticle tracking analyser (PARTICLE METRIX, ZetaVIEW), and their morphologies were characterised by transmission electron microscope (TEM) (Hitachi, HT-7700).

2.12 | Proteomic Analysis

A total of 50 µg protein derived from EVs were subjected to proteomic analysis using an EASY nLC 1000 coupled with an C18 analytical column (1.9 µm, 75 µm*20 cm) at a flow rate of 200 nL/min. Raw data were analysed with Proteome Discoverer v2.4 software (Thermo Fisher, Waltham, MA, USA) using label-free quantitation. The resolution for MS and MS/MS data searches was 10 ppm and 0.05 Da, respectively. Two missed trypsin cleavages and modifications of M-oxidation, KR-deamidation, ST-dehydration, and STY-phosphorylation were permitted. Peptide identifications were filtered at <1% and <5% FDR cutoffs. The human UniProt dataset (639,722 entries) was used for data alignment. Fold-change ratios between groups were obtained by matched peptide-based label-free quantitation, with *p* value calculated by the Benjamini–Hochberg correction for FDR. Differentially expressed proteins were identified with a fold-change greater than 1.2 and *p* value less than 0.05. Their biological functions were annotated using GO pathway and GSEA analysis.

2.13 | ChIP-qPCR

ChIP analysis of Nrf2 binding elements within the SDC4 gene body was performed using the Pierce Magnetic ChIP Kit (Thermo Scientific, cat#26157). Briefly, cells were fixed with 1% formaldehyde for 10 min and then incubated with 0.125 M glycine for 5 min to quench the fixation. Subsequently, cells were harvested for lysis and MNase digestion following the manufacturer's illustration. The supernatant was collected and incubated with Nrf2 antibody (dilution: 1:200) overnight at 4°C, followed by reacting with ChIP Grade Protein A/G Magnetic Beads for 2 h at 4°C with gentle mixing. The beads were then washed three times with IP wash buffer 1 and once with IP wash buffer 2. The DNA-protein complexes were eluted in IP Elution Buffer and cross-linking was reversed by incubating at 65°C for 1.5 h. The bound DNA was extracted and quantified by qPCR. DNA immunoprecipitated with IgG served as a negative control, while DNA immunoprecipitated with Anti-RNA Polymerase II served as a positive control. Primers used for ChIP-qPCR are listed in Table S3.

2.14 | EV Labelling and Immunofluorescence

EVs were labelled using PKH67 Green Fluorescent Cell Linker Kit (Sigma, cat#PKH67GL). In brief, EVs were resuspended in 100 µL PBS and 100 µL of Diluent C containing 1:250 diluted PKH67 was added. The mixture was gently pipetted for 30 s and incubated at room temperature for 5 min. Staining was stopped by adding 200 µL of 1% BSA-PBS. The volume was adjusted to 3.5 mL with serum-free media. The EV suspension was layered on top of a 0.971 M sucrose (in PBS) gradient and centrifuged at $190,000 \times g$ for 2 h to pellet the EVs while retaining the unbound dye on top of the sucrose layer. The pelleted EVs were resuspended in PBS, centrifuged at $100,000 \times g$ and then resuspended in PBS for particle concentration normalisation by Nanoparticle Tracking Analysis (NTA). A total of 1×10^6 particles of PKH67-labelled EVs were incubated with 5×10^4 A549 cells for 24 h. After incubation, cells were fixed with 4% paraformaldehyde, permeabilised with 0.2% Triton X-100 and blocked with 3% bovine serum albumin (BSA) for 20, 15 and 30 min, respectively. Cells were then stained with anti-Syndecan 4 antibody and subsequently with Alexa Fluor 568 goat anti-rabbit IgG. Nuclei were counterstained with DAPI. Fluorescent images were acquired using a Nikon Eclipse Ti2 inverted microscope with AX confocal system. Pearson's colocalisation coefficient and Mander overlap coefficient were calculated using NIS-Elements software to assess the overlap between PKH67-labelled EVs and SDC4 protein.

2.15 | *SDC4* knockdown and Overexpression

Three different small interfering RNA (siRNA) targeting *SDC4* and a negative control siRNA were purchased from Integrated DNA Technologies, Inc. (TriFECTa DsiRNA Kit, cat#hs.Ri.SDC4.13). One day prior to transfection, 1,4-D-transformed WT cells were plated. Transfection was performed with *SDC4* siRNA at a final concentration of 50 nM using Lipofectamine 2000. For *SDC4* overexpression, the human SDC4 gene was cloned into the pcDNA3.1-HA vector (Addgene#128034), with the primers used listed in Table S4. The empty vector served as a negative control. Both plasmids were transfected into 1,4-D-transformed Nrf2 KO cells using Lipofectamine 2000. Cells were harvested 72-h post-transfection, and cellular proteins and cell culture supernatants were collected for further analysis.

2.16 | Benchmark Dose Analysis

Dose-response analysis was conducted using the US EPA's Benchmark Dose Software (BMDS v3.3.2) (EPA 2023). Benchmark response (BMR) values of 10% extra risk and their corresponding 95% lower confidence limits ($BMDL_{10}$) were calculated to evaluate the intensity of 1,4-D toxicity on cells. A lower BMD_{10} value indicates higher sensitivity to 1,4-D treatment.

2.17 | Statistical Analysis

All experiments were performed independently in triplicate with at least three biological replicates, unless otherwise specified. Inter-group differences were analysed by Student's *t*-test or one-way analysis of variance (ANOVA). All statistical analyses were two-sided with a significance level set at $p < 0.05$. Statistical analyses were conducted using GraphPad Prism 7 software (GraphPad Software, San Diego, CA).

3 | Results

3.1 | 1,4-D Activates Nrf2 in a Dose-Dependent Manner

To investigate whether 1,4-D at environmentally relevant concentration is capable of inducing Nrf2 activation, WT and Nrf2 KO BEAS-2B cells were treated with 0–20 ppm 1,4-D for 6 h. We observed a dose-dependent activation of Nrf2 by 1,4-D in WT cells. However, in Nrf2 KO cells, no active Nrf2 was detected, except for a non-specific protein possibly resulted from CRISPR-Cas9 gene editing (Figure 1A). Given that AHR is a known sensor for xenobiotics through transcriptional regulation of the phase I enzymes, primarily the CYP enzymes (Larigot et al. 2018), we further examined the impact of 1,4-D on AHR activation. In both WT and Nrf2 KO cells, 1,4-D treatment led to a dose-dependent decrease in AHR protein abundance (Figure 1A). Additionally, we observed a notable increase in phosphorylated JNK (pJNK) following Nrf2 knockout, indicating a heightened cellular stress response. In contrast, the activation effect of 1,4-D on JNK appeared to be marginal (Figure 1A). Immunofluorescent

staining with DAPI and Nrf2 revealed nuclear translocation of Nrf2 in WT cells treated with 1,4-D for 6 h, highlighting the role of Nrf2 as a transcription factor (Figure 1B). To better illustrate this, we performed nucleus extraction and fractionation followed by Nrf2 protein detection. As shown in Figure 1C, the intensity of Nrf2 in the nucleus increased in a dose-dependent manner when WT cells were treated with 1.25–20 ppm 1,4-D for 6 h, indicating robust Nrf2 activation. In contrast, the Nrf2 signal in the cytoplasm showed no significant change, reinforcing Nrf2's role as a transcription factor in the 1,4-D toxicity response. In an Nrf2 luciferase reporter assay, 12 h of 1,4-D treatment significantly enhanced ARE activity (Nrf2 activity), comparable to the positive control (0.25–4 µM arsenic treated for 12 h) (Figure 1D). However, its effect on AHR activity remained inconclusive relative to the Kynurenine group, where cells were treated with 2.5–640 µM Kynurenine for 12 h (Figure 1E). This aligns with the findings of Lafranconi et al. (2023), who reported that 1,4-D does not activate AHR. We also explored the impacts of Nrf2 deletion on cell survival. Benchmark dose (BMD) analysis revealed similar cytotoxicity profiles between WT (BMD_{10}: 0.14 ppm) and Nrf2 KO (BMD_{10}: 0.13 ppm) cells after 24 h of 1,4-D treatment (Figure 1F, left panel). However, extending the treatment duration to 48 h significantly increased the cytotoxicity of 1,4-D in Nrf2 KO cells (BMD_{10}: 0.08 ppm), whereas WT cells exhibited notable recovery from cytotoxicity at 1,4-D concentrations ranging from 0.31 to 20 ppm (BMD_{10}:17.47 ppm) (Figure 1F, right panel). Furthermore, to determine if continuous 1,4-D treatment would sustain Nrf2 activation, we treated WT cells with 0–20 ppm 1,4-D for 2 months. The results showed stable 1,4-D-dependent Nrf2 activation in WT cells (Figure 1G). Collectively, these results indicate that 1,4-D consistently activates Nrf2 in a dose-dependent manner, and that Nrf2 knockout reduces cell survival and impairs recovery from 1,4-D-induced toxicity.

3.2 | Nrf2 Dependency of 1.4-D-Induced Malignant Transformation

Given the oncogenic property of Nrf2 suggested by numerous studies (Sporn and Liby 2012), we monitored surrogate markers for tumour initiation, including anchorage-independent colony formation assay in soft agar, plate clonogenic growth, migration and invasion in WT and Nrf2 KO cells following 2-month treatment with 0–20 ppm 1,4-D. The soft agar colony formation assay showed that 1,4-D treatment increased colony formation in both WT and Nrf2 KO cells (Figure 2A). However, the extent of colony formation induced by 1,4-D was significantly reduced in Nrf2 KO cells compared to WT cells (Figure 2A). 1,4-D-transformed WT cells exhibited large colony formation, with cell numbers 2.35- to 3.80-fold greater than those in 1,4-D-transformed Nrf2 KO cells, as corroborated by the plate clonogenic growth assay (Figure 2B). A notable decrease in migration and invasion potential induced by 1,4-D was observed in Nrf2 KO cells compared to WT cells (Figure 2C). Furthermore, we conducted mouse xenograft experiment to examine the tumorigenicity of 1,4-D. Mice developed in-situ tumours 8 and 10 weeks after receiving a subcutaneous injection of 1,4-D-transformed WT and Nrf2 KO cells, respectively, with tumour formation rate of 100% (5/5) in 1,4-D-transformed WT group and 80% (4/5) in 1,4-D-transformed Nrf2 KO group (Figure 2F). Compared to the 1,4-D-transformed
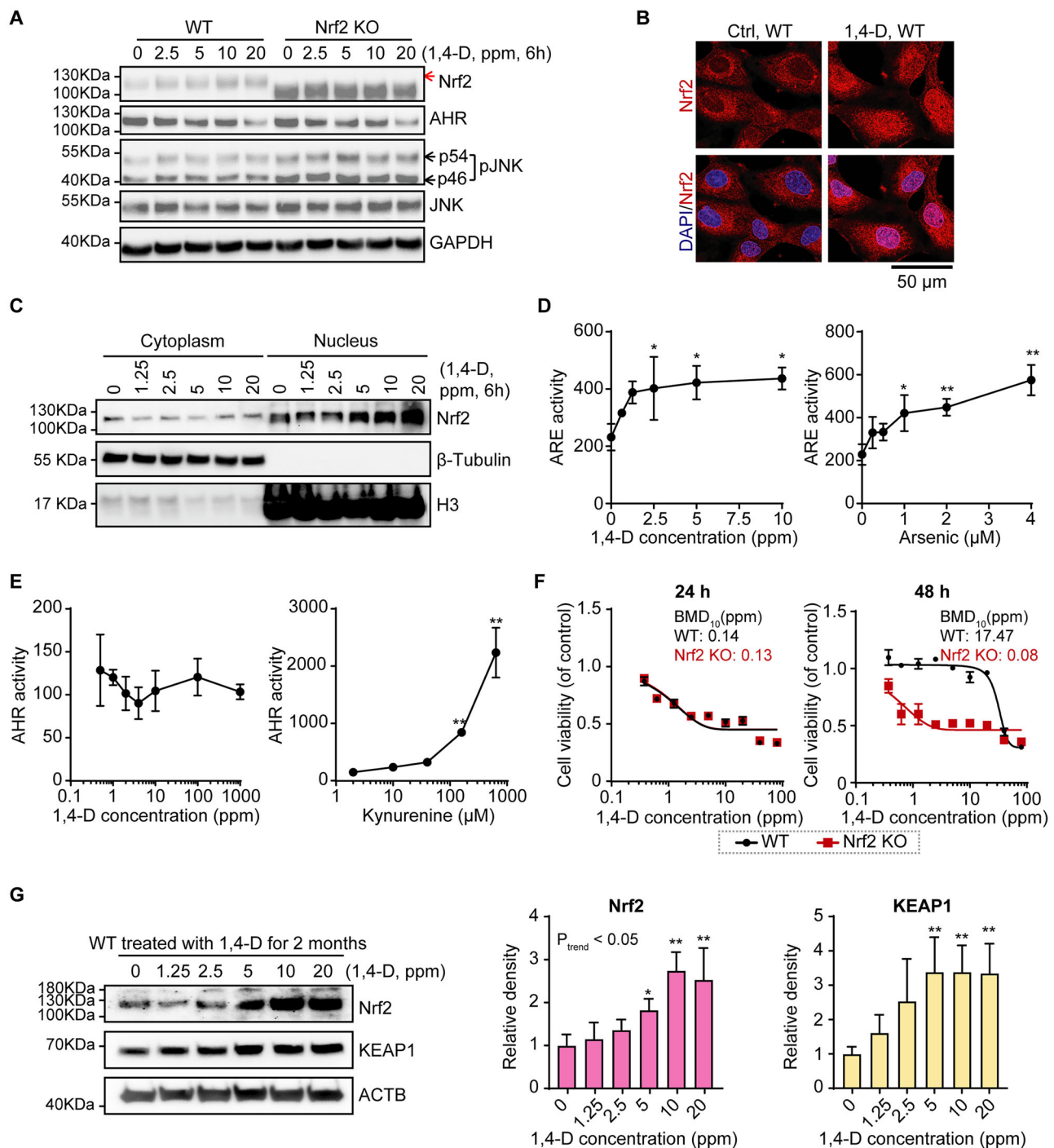
FIGURE 1 | 1,4-D consistently activates Nrf2 in BEAS-2B cells. (A) Representative immunoblots showing the expression levels of Nrf2, AHR, pJNK, JNK and GAPDH in WT and Nrf2 KO cells treated with 1,4-D at concentrations ranging from 0 to 20 ppm for 6 h. (B) Photomicrographs illustrating the nuclear translocation of Nrf2 in WT cells treated with 20 ppm 1,4-D. (C) Cytoplasmic and nuclear fractionation showing a dose-dependent increase in Nrf2 nuclear translocation in WT cells treated with 1,4-D (0–20 ppm) for 6 h. (D) ARE-inducible luciferase reporter assay demonstrating the dose-dependent Nrf2 activation after 12 h of treatment with the indicated concentrations of 1,4-D (left), and inorganic arsenic (0.25–4 µM) as a positive control (right). Data are presented as mean ± SD, $n = 6$, $*p < 0.05$, $**p < 0.01$ vs. control (one-way ANOVA with Bonferroni's multiple comparisons test). (E) AHR luciferase reporter activity assay showing WT cells treated with 1,4-D at the indicated concentrations for 12 h (left), with kynurenine (2.5–640 µM) as a positive control (right). Data are expressed as mean ± SD, $n = 6$, $**p < 0.01$ vs. control (one-way ANOVA with Bonferroni's multiple comparisons test). (F) Cytotoxicity profiles of 1,4-D in WT and Nrf2 KO cells, modelled using Benchmark Dose (BMD) analysis, with $BMDL_{10}$ values indicating the cytotoxicity threshold. (G) Immunoblots showing the expression of Nrf2, KEAP1, and ACTB in WT cells treated with 0 to 20 ppm 1,4-D for 2 months, with their quantitative results shown in the right panel. Data are presented as mean ± SD, $n = 3$, $*p < 0.05$, $**p < 0.01$ vs. control (one-way ANOVA and trend analysis).
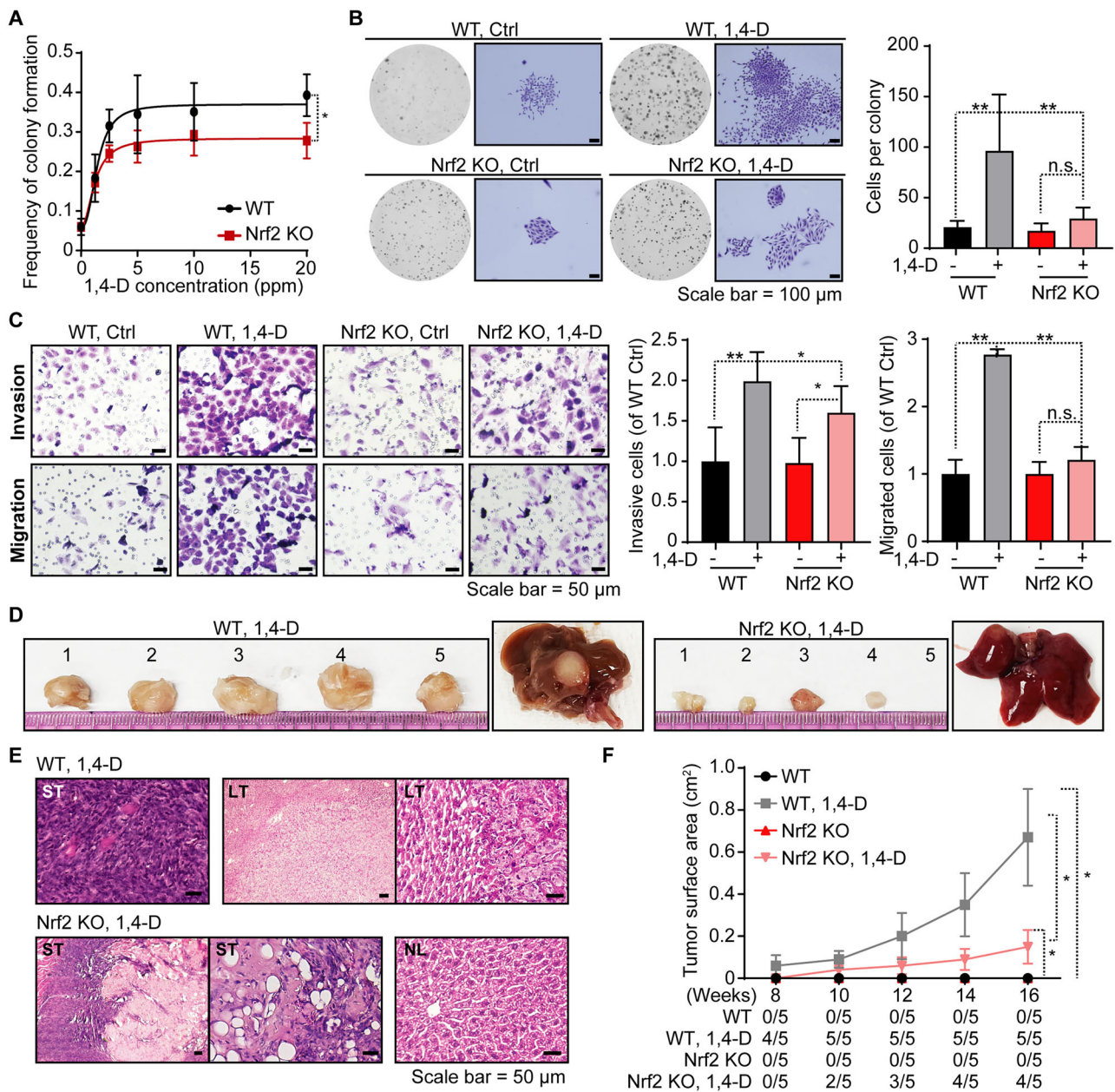
FIGURE 2 | Knockout of Nrf2 reduces 1,4-D-induced malignancy transformation. (A) Soft agar colony formation of WT and Nrf2 KO cells treated with 1.25 to 20 ppm 1,4-D for 2 months. Data are expressed as mean ± SD, $n = 6$, *$p < 0.05$ vs. control (paired Student's *t* test). (B) Representative images of colony morphology from plate clonogenic growth assay, with quantification of the number of cells per colony. Data are expressed as mean ± SD, $n = 10$, **$p < 0.01$ vs. the corresponding control (one-way ANOVA with Bonferroni's multiple comparisons test). (C) Representative images showing changes in the invasion and migration capabilities of WT cells and Nrf2 KO cells treated with 1,4-D for 2 months, with quantification of invasive or migrated cells. Data are presented as mean ± SD, $n = 10$, **$p < 0.01$, *$p < 0.05$ vs. control (one-way ANOVA with Bonferroni's multiple comparisons test). (D) Photographs of subcutaneous tumours and representative liver samples from the mice injected with 1,4-D-transformed WT and Nrf2 KO cells. The 1,4-D-transformed WT cells formed larger tumours and displayed liver metastasis, while Nrf2 KO cells showed reduced tumour size and no metastasis. (E) Histological analysis of primary tumours and liver metastasis from mice received with 1,4-D-transformed WT and Nrf2 KO cells. ST: subcutaneous tumour; LT: liver tumour; NL: normal liver. (F) Time-dependent quantification of tumour size. Tumour formation rate at corresponding time points were shown below. Data are presented as mean ± SD. $n = 5$, *$p < 0.05$ vs. control (paired one-way ANOVA with Bonferroni's multiple comparisons test).

Nrf2 KO group, mice injected with 1,4-D-transformed WT cells developed tumours with larger volume, faster growth rates and higher pathological malignancy (Figure 2D–F). Additionally, liver metastasis was observed in 2 out of 5 mice injected with 1,4-D-transformed WT cells (Figure 2D,E). In contrast, no visible metastatic tumours of the 1,4-transformed Nrf2 KO cells were detected. Taken together, these results reveal the carcinogenic properties of 1,4-D at environmentally relevant concentrations, highlighting its dependency on Nrf2 activation.
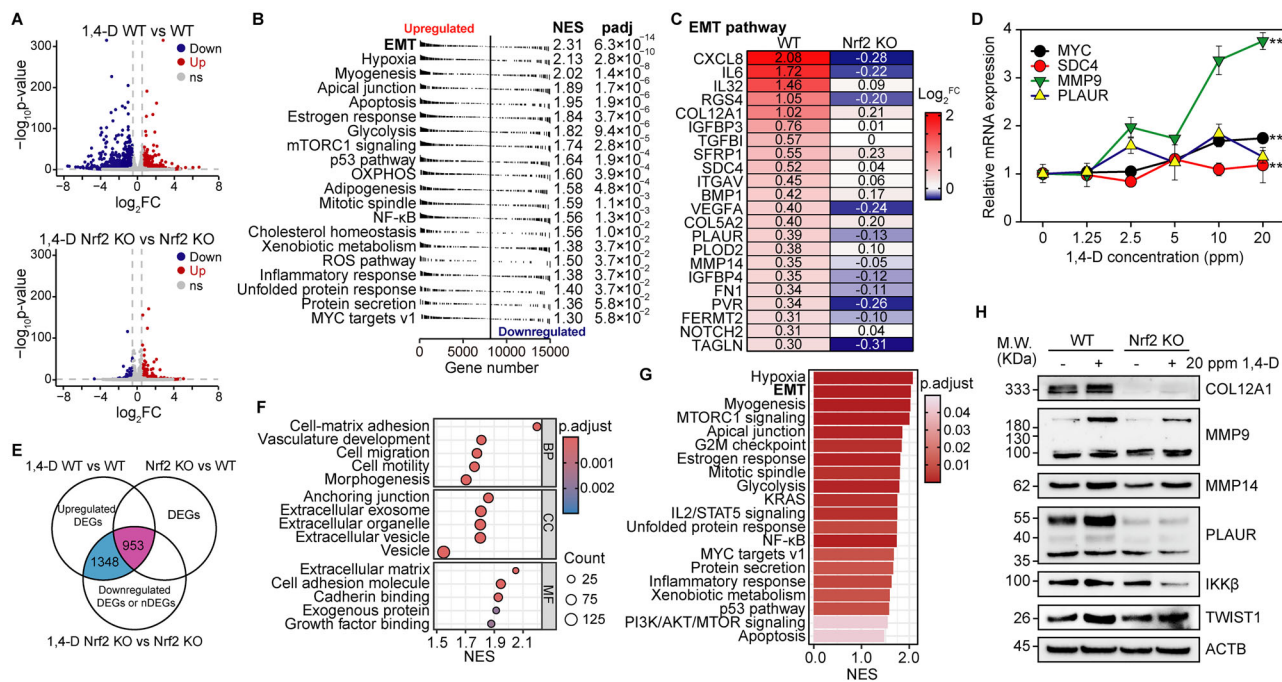
FIGURE 3 | Nrf2 mediates EMT process and EV biogenesis induced by 1,4-D. (A) Volcano plots illustrating differentially expressed genes (DEGs) induced by 1,4-D in transformed WT and Nrf2 KO cells. Significantly upregulated and downregulated genes in response to 1,4-D treatment are highlighted. (B) GSEA based on the Hallmark collection showing the Top 20 pathways enriched in 1,4-D-transformed WT cells. NES: normalised enrichment score. (C) The expression of key genes in the EMT pathway is upregulated by 1,4-D in WT cells but diminished in Nrf2 KO cells. RNA-seq results are shown as log2 fold changes. (D) qRT-PCR results showing the expression levels of *MYC*, *SDC4*, *MMP9* and *PLAUR* in 1,4-D-transformed WT cells. Data are presented as mean ± SD. $n = 6$, $**p < 0.01$ vs. control (one-way ANOVA with trend analysis). (E) Venny diagram illustrating 2031 of 1,4-D-induced, Nrf2-dependent genes, upregulated in WT cells treated with 1,4-D but either downregulated or non-responsive in Nrf2 KO cells. Of these, 953 genes were differentially expressed between untreated WT and Nrf2 KO cells. nDEGs: non-differentially expressed genes. (F) GO pathway analysis of the 953 genes showing the involvement in the regulation of EV biogenesis. BP: biological process; CC: cellular component; MF: molecular function. (G) GSEA highlights the role of the 953 genes in mediating the EMT process in 1,4-D-transformed WT cells. (H) Immunoblots showing the expression of COL12A1, MMP9, MMP14, PLAUR, IKKβ, TWIST1 and ACTB in WT and Nrf2 KO cells transformed by 20 ppm 1,4-D.

3.3 | 1,4-D Induces Genes Associated With EMT and EV Biogenesis in an Nrf2-dependent Manner

To investigate the molecular determinants of 1,4-D-induced malignancy and the role of Nrf2 in this process, we profiled the DEGs between 1,4-D-transformed WT and 1,4-D-transformed Nrf2 KO cells, alongside corresponding control cells. As depicted in Figure 3A, 1,4-D treatment significantly altered the expression of 7629 genes in WT cells (Figure 3A, top), a 1.42-fold increase compared to the 5390 genes affected in Nrf2 KO cells (Figure 3A, bottom). This difference was even more pronounced in the downregulated gene set, with a 1.78-fold increase in WT cells. Subsequently, we performed GSEA on the DEGs in the WT cell group to explore the key pathways involved in 1,4-D-induced malignancy. The results revealed that the EMT pathway was one of the most affected pathways (Figure 3B). The top 20 pathways were closely associated with xenobiotic metabolism, oxidative stress, cell cycle regulation and carcinogenesis, further confirming the carcinogenic potential of 1,4-D (Figure 3B). Additionally, 1,4-D-transformed WT cells showed increased expression of EMT target genes (*CXCL8*, *COL12A1*, *SDC4* and *MMP14*), while those genes were downregulated by 1,4-D in Nrf2 KO cells (Figure 3C). The induction of several genes in the EMT pathway was confirmed through qRT-PCR (Figure 3D). *MYC*, *SDC4* and *MMP9* exhibited dose-dependent induction by 1,4-D, highlighting

the predominant role of the EMT pathway in 1,4-D-induced cell malignancy. To further address the oncogenic role of Nrf2, we then focused on identifying genes that were upregulated by 1,4-D in WT cells but either downregulated or non-responsive in Nrf2 KO cells. Out of 2301 genes showing 1,4-D-induced and Nrf2-dependent, 953 met the criteria for DEGs between Nrf2 KO and WT cells without 1,4-D treatment (Figure 3E). The top-induced 30 genes are listed in Figure S1, with several, such as *APOD* (Ashida et al. 2004), *WNT11* (Uysal-Onganer et al. 2010) and *MMP9* (Kaplan et al. 2005), previously reported as oncogenes. GO pathway analysis showed that most of 953 genes were related to biological processes such as cell-matrix adhesion, vasculature development and cell migration (Figure 3F). Intriguingly, the proteins encoded by these genes were primarily involved in regulating the extracellular matrix and cell adhesion, particularly through EV-mediated pathways (Figure 3F). According to the Vesiclepedia database (Chitti et al. 2024), 79.01% (753/953) of these Nrf2-dependent proteins were reported to be loaded into EVs or to play a role in EV biogenesis and function (Table S5). Additionally, the EMT pathway was identified as the second most significantly enriched among these 953 genes (Figure 3G). Furthermore, the Nrf2 dependency of several EMT-related proteins were verified by Western blotting, showing that the protein abundance of COL12A1, MMP9, MMP14, PLAUR, IKKβ and TWIST1 was significantly induced by 1,4-D but diminished upon Nrf2

knockout (Figure 3H). The expression changes were consistent with our transcriptomic findings, reinforcing the reliability of our RNA sequencing results and emphasising the critical role of Nrf2 activation in 1,4-D-induced malignant transformation. Collectively, these findings underscore the pivotal role of Nrf2 in mediating EMT induced by 1,4-D, with EVs likely playing a key role in this process.

3.4 | Nrf2-Dependent EVs Induced by 1,4-D Promote EMT Phenotypes in Recipient Cells

In our initial testing of the cellular response to transient 1,4-D treatment, we noted a pronounced Nrf2-dependent induction of genes associated with EV biogenesis and release (data not shown), which aligns with the top enrichment of EV-related pathways in the 1,4-D-transformed cells (Figure 3F). To directly assess the impact of 1,4-D on EV generation, we isolated EVs from the culture media of WT cells, 1,4-D-transformed WT cells, Nrf2 KO cells and 1,4-D-transformed Nrf2 KO cells using differential ultracentrifugation. The purity of the isolated EVs was confirmed by Western blotting for the EV surface marker Alix (PDCD6IP) and the endoplasmic reticulum (ER) protein calnexin (CANX) (Figure 4A). We also analysed the protein abundance of CD82 and CD9, which are part of the 1,4-D-induced, Nrf2-dependent gene set, and observed similar enrichment patterns in EVs (Figure 4A). Existing literature suggests that changes in EV concentration can mediate downstream effects. Our previous results suggested that 1,4-D activated cholesterol metabolism, the unfolded protein response (Figure 3B), and several GTPase family members (e.g., RAB38, RAB22A, ABCE1, RALA and SLC12A2) (data not shown), highlighting the potential role of EVs in 1,4-D-induced cell transformation. To further investigate this connection, we characterised the impact of 1,4-D on EV size, number, morphology and functions. Representative TEM images revealed that over 80% of EVs exhibited a clear lipid bilayer/membrane with electron dense cargo in the lumen. Nearly all EVs from WT cells were intact, round-shaped, and had a median size of 138 nm (Figure 4B). Some EVs from 1,4-D-transformed WT cells showed membrane discontinuities (Figure 4B). Additionally, 1,4-D induced the formation of numerous sac-like vesicles without a clear lipid bilayer, ranging from 500 to 800 nm in size, in WT cells (Figure 4B,E). EVs from Nrf2 KO cells were visibly smaller, with a median size of 119 nm, compared to those from WT cells (Figure 4B), while EVs from 1,4-D-transformed Nrf2 KO cells displayed membrane roughness (Figure 4B). NTA revealed that 1,4-D treatment significantly increased EV release in both WT and Nrf2 KO cells (Figure 4C), with a more pronounced fold increase in WT cells compared to Nrf2 KO cells (Figure 4D). Coupling TEM images with NTA results, the high peaks of EVs at sizes of 500 and 800 nm in 1,4-D-transformed WT cells likely corresponded to sac-like vesicles lacking a clear lipid bilayer (Figure 4B,E). Large-sized EVs (>500 nm) were significantly reduced in 1,4-D-transformed Nrf2 KO cells, while they significantly increased in 1,4-D-transformed WT cells (Figure 4E,F). To assess whether EVs promote EMT, we incubated A549 lung tumour cells with the collected cell culture medium containing EVs for 24 h. EVs from 1,4-D-transformed WT cells showed the strongest potential to enhance the proliferation, migration and invasion of A549 cells (Figure 4G–J). In contrast, EVs from 1,4-D-transformed Nrf2 KO cells had no discernible effect on A549 cells (Figure 4G–

J). Collectively, these findings suggest that Nrf2-dependent EVs induced by 1,4-D promote the EMT phenotypes in recipient cells.

3.5 | Nrf2 Activation Induced by 1,4-D Promotes the Loading of EMT-Related Proteins Into EVs

Many studies have indicated an association between EV secretion and various biological endpoints. However, the physical characteristics of EVs did not fully align with our expectations, as 1,4-D significantly increased EV numbers, whereas Nrf2 knockout weakened this effect. Importantly, these findings offer a new perspective, suggesting that EVs carrying oncogenic or EMT-promoting cargo may contribute to this process. To further investigate how Nrf2 activation influences the EMT characteristics of recipient cells via 1,4-D-induced EVs, we performed cell and EV proteomics. Following 1,4-D treatment, we identified 1610 and 1792 differentially expressed proteins in WT and Nrf2 KO cells, respectively. Among these, 359 proteins that were downregulated in 1,4-D-transformed Nrf2 KO cells overlapped with those upregulated in 1,4-D-transformed WT cells, with significant enrichment in ROS and fatty acid metabolism pathways (Figure 5A). Additionally, we identified 918 and 544 differentially expressed proteins in EVs from WT and Nrf2 KO cells, respectively, following 1,4-D treatment. Notably, 31.8% (173 proteins) of the downregulated proteins in EVs from 1,4-D-transformed Nrf2 KO cells overlapped with those upregulated in EVs from 1,4-D-transformed WT cells, indicating that the induction of these EV proteins by 1,4-D is Nrf2 dependent (Figure 5B). GSEA of these EV proteins revealed that the MYC and EMT pathways were the top 2 enriched pathways (Figure 5B). The expression levels of these Nrf2-dependent EV proteins in the EMT pathway were depicted in Figure S2. Several EMT-associated proteins, such as SFRP1, MMP14, SDC4 and COL12A1, were also enriched in the EMT pathway based on RNA-seq profiles (Figure 3C). Moreover, overlapping 1,4-D-induced Nrf2-dependent proteins between the EV and cell proteomes showed significant enrichment in ROS pathways (Figure 5C). Integrative analysis of cell and EV proteomics with cell transcriptomics revealed that the 1,4-D-induced, Nrf2-dependent genes overlapping between EV proteomics and cell transcriptomics (but not between cell proteomics and cell transcriptomics) were significantly enriched in the EMT pathway. This further confirms the EMT-promoting effect of EVs (Figure 5D). We also identified several 1,4-D-induced, Nrf2-dependent proteins associated with EMT propagation that were significantly enriched in EVs, including MMP14, SDC4 and COL12A1 (Figure 5E). To assess their functional relevance, we examined their abundance in A549 recipient cells after 24-h EV treatment (Figure 5F). EVs from 1,4-D-transformed WT cells significantly increased SDC4 and COL12A1 levels, whereas Nrf2 knockout attenuated 1,4-D-induced SDC4 expression and reduced baseline COL12A1 levels. Interestingly, CAPG protein abundance remained unchanged upon 1,4-D treatment but was significantly downregulated in A549 cells treated with EVs from 1,4-D-transformed Nrf2 KO cells compared to the Nrf2 control group. Meanwhile, NNMT expression exhibited only a marginal increase in the 1,4-D-transformed WT cell group. Notably, the changes in these four proteins in A549 cells were highly consistent with their trends in EVs (Figure 5C,F). Additionally, we examined key EMT-related proteins (MMP14, SLUG, NANOG, VIM and TWIST1) in A549 cells following EV treatment (Figure 5F). EVs
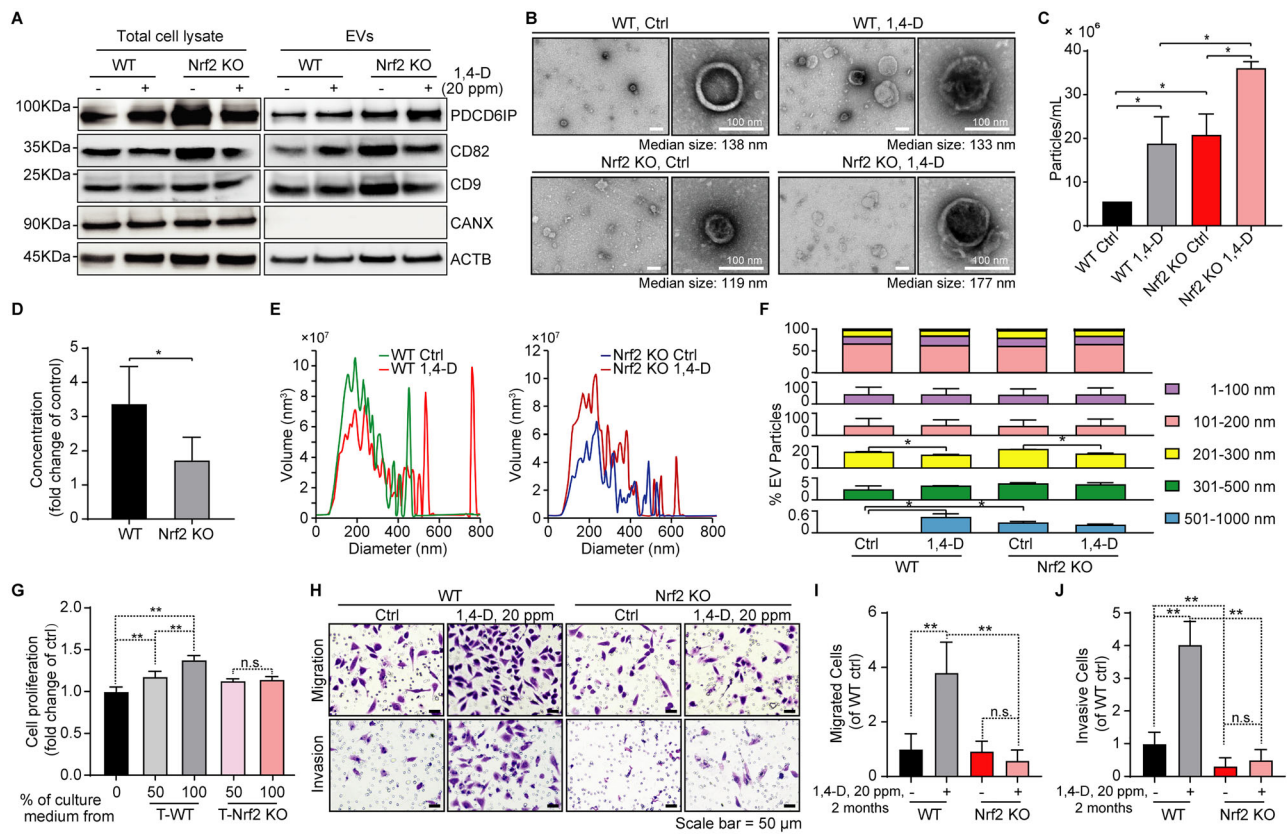
FIGURE 4 | Characterisation and function analysis of 1,4-D-induced EVs in WT and Nrf2 KO cells. (A) Immunoblots showing the expression of PDCD6IP, CD82, CD9, CANX and ACTB in cell lysates and EV samples derived from WT, 1,4-D-transformed WT, Nrf2 KO and 1,4-D-transformed Nrf2 KO cells. (B) Representative TEM photographs of EVs from the indicated groups. (C and D) EV concentrations across the groups, with 1,4-D-induced changes in EV production in WT and Nrf2 KO cells shown as fold changes. Data are presented as mean ± SD, $n = 3$, *$p < 0.05$ vs. control (one-way ANOVA with Bonferroni's multiple comparisons test). (E and F) Size distribution of EVs in each group, determined and quantified using NTA. Data are presented as mean ± SD, $n = 3$, *$p < 0.05$ vs. control (one-way ANOVA with Bonferroni's multiple comparisons test). (G) Effects of EVs from 1,4-D-transformed WT (T-WT) and 1,4-D-transformed Nrf2 KO (T-Nrf2 KO) cells on A549 cell proliferation. Data are presented as mean ± SD, $n = 6$, **$p < 0.01$ vs. control (one-way ANOVA with Bonferroni's multiple comparisons test). (H–J) Representative images illustrating changes in migration and invasion capabilities of A549 cells treated with EVs from the indicated groups, with quantification of migrated or invasive cells. Data are presented as mean ± SD, $n = 10$, **p < 0.01 vs. control (one-way ANOVA with Bonferroni's multiple comparisons test).

from 1,4-D-transformed WT cells significantly upregulated SLUG and NANOG, with a marginal increase in TWIST1, whereas EVs from 1,4-D-transformed Nrf2 KO cells decreased MMP14 and VIM abundance. These protein alterations correlate with the observed EMT phenotype changes in A549 cells, further supporting their functional relevance (Figure 4G–J). Collectively, our data illustrates that Nrf2 activation by 1,4-D promotes the loading of EMT-related proteins into EVs, thereby influencing the EMT phenotypes of recipient cells.

3.6 | Nrf2 Modulates the 1,4-D-Induced EMT Process via SDC4-Enriched EVs

Emerging evidence has highlighted the critical role of SDC4 in cancer cell motility, invasion, and tropism (Agere et al. 2018; Vuoriluoto et al. 2011). Here, we observed that SDC4 expression is induced by 1,4-D in an Nrf2-dependent manner, as evidenced by our cell RNA-seq data and EV proteome analysis (Figures 3C and S2). Notably, SDC4 was the only EV surface biomarker among EMT-related proteins responsive to 1,4-D exposure, providing

new insights into the identification of functional EVs involved in EMT regulation (Figure 6A). To further validate its role, we assessed SDC4 protein abundance in EVs secreted by the equal numbers of cells, confirming its Nrf2 dependency and inducibility by 1,4-D (Figure 6B). Moreover, a dose-dependent increase in SDC4 expression was observed in 1,4-D-transformed WT cells (Figure 6C). We also examined SDC4 levels in EVs derived from 1,4-D-transformed WT and Nrf2 KO cells, which were generated by exposing cells to 1.25–20 ppm 1,4-D for 2 months. Our results showed a dose-dependent upregulation of SDC4 in EVs from transformed WT cells, particularly in response to 5–10 ppm of 1,4-D exposure (Figure 6D). However, in EVs from 1,4-D-transformed Nrf2 KO cells, SDC4 upregulation was observed only at intermediate doses (2.5, 5 and 10 ppm), while its expression was lower at both the lowest (1.25 ppm) and highest (20 ppm) doses (Figure 6D). This pattern suggests that Nrf2 plays a key role in regulating SDC4 loading into EVs in response to 1,4-D exposure. To investigate the functional relevance of SDC4 in EMT propagation of recipient cells, we performed PKH67 staining on EVs derived from WT, 1,4-D-transformed WT, Nrf2 KO, 1,4-D-transformed Nrf2 KO cells. These labelled EVs were then
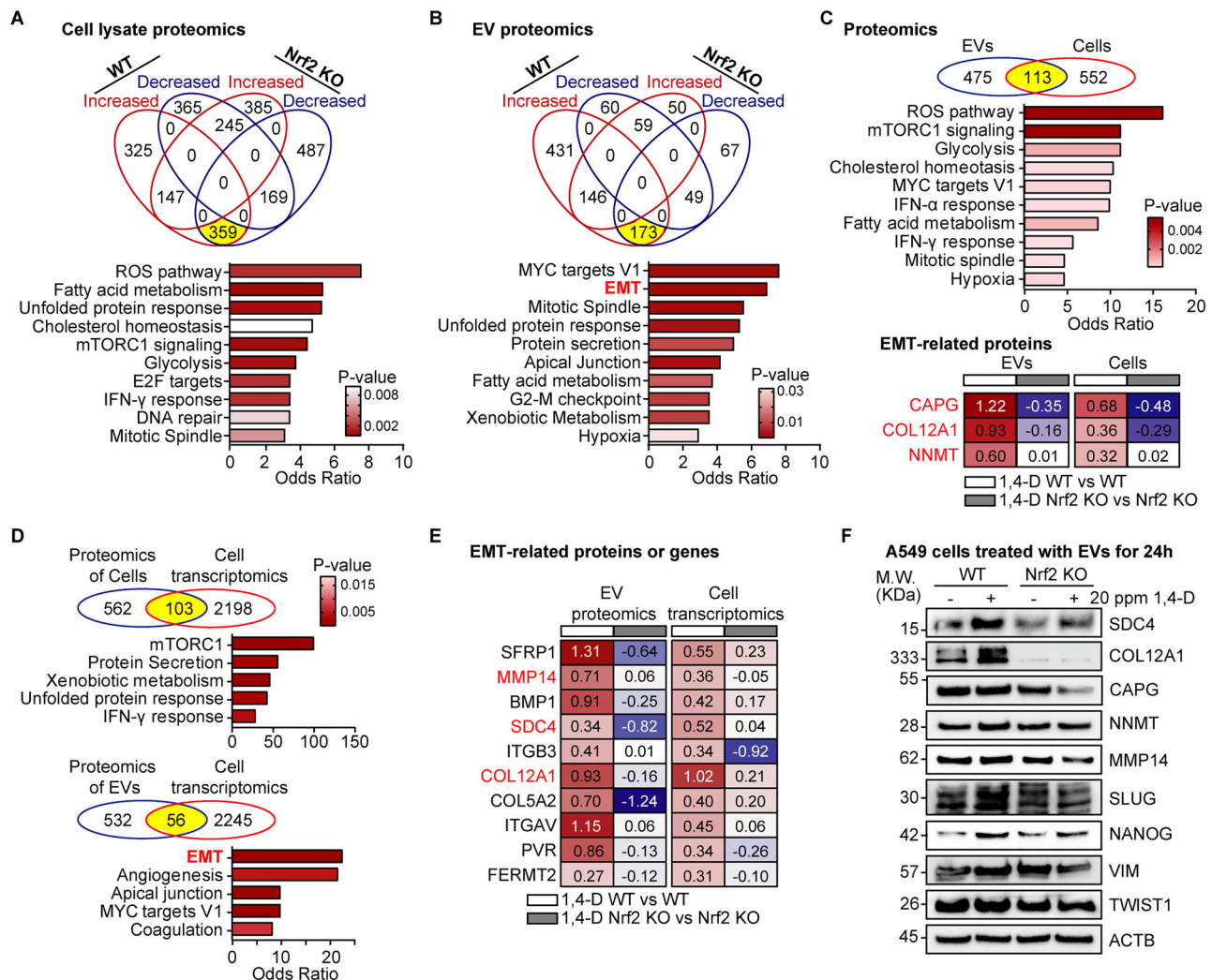
FIGURE 5 | Nrf2 activation induced by 1,4-D promotes EMT protein loading in EVs. (A) Venn diagram illustrating 359 1,4-D-induced, Nrf2-dependent proteins identified in cell lysate proteomics, significantly enriched in ROS and fatty acid metabolism pathways. (B) Venny diagram illustrating 173 1,4-D-induced, Nrf2-dependent proteins identified in EV proteomics, significantly enriched in the MYC and EMT pathways. (C) Overlapping proteins between the EV and cell proteomes are significantly enriched in ROS, mTORC1 signalling and glycolysis pathways. A heatmap illustrates the abundance of overlapped 1,4-D-induced, Nrf2-dependent proteins in EVs and cell lysates, which are also associated with EMT. Protein abundances are shown as log2 fold changes. (D) Pathway enrichment analysis (Hallmark collection) reveals significant enrichment of the EMT pathway among genes overlapping between the EV proteome and cell transcriptome. (E) Heatmap displaying the protein abundance and gene expression of SFRP1, MMP14, BMP1, SDC4, ITGB3, COL12A1, COL5A2, ITGAV, PVR and FERMT2 in EV samples and cells. These proteins are expressed in a 1,4-D-induced, Nrf2-dependent manner and are significantly enriched in the EMT pathway. Data are shown as log2 fold changes. (F) Representative immunoblots showing the abundance of SDC4, COL12A1, CAPG, NNMT, MMP14, SLUG, NANOG, VIM, TWIST1 and ACTB in A549 recipient cells following 24-h EV treatment.

incubated with A549 cells for 24 h, followed by SDC4 staining. We observed that EVs from 1,4-D-transformed WT cells were significantly internalised by A549 cells, leading to an increased abundance of SDC4, both from the EVs themselves and through its induction in A549 cells (Figures 5F and 6E). Notably, the highest Pearson's correlation coefficient and Mander overlap coefficient between PKH67 and SDC4 were found in the 1,4-D-transformed WT cell group (Figure 6F), indicating the greatest spatial overlap of these two proteins. Collectively, these findings suggest that SDC4 is a key Nrf2-dependent EV cargo involved in 1,4-D-induced EMT, further underscoring its potential as a biomarker for functional EVs mediating EMT propagation in recipient cells.

3.7 | SDC4 Is a Nrf2 Target Gene for 1,4-D-Induced Cell Migration and Invasion

As noted above, 1,4-D significantly increased SDC4 abundance in EVs from WT cells, whereas Nrf2 knockout attenuated this effect (Figure 6B,D). Based on this observation, we hypothesise that Nrf2 activation enhances *SDC4* expression and promotes the release of SDC4-enriched EVs, thereby accelerating EMT progression. To test this hypothesis, we first examined the Nrf2 enrichment at the SDC4 gene locus using our Nrf2 ChIP-seq files from a previous arsenic carcinogenesis study. Our analysis revealed clusters of Nrf2 binding peaks across the SDC4 gene body, particularly spanning the transcription start site
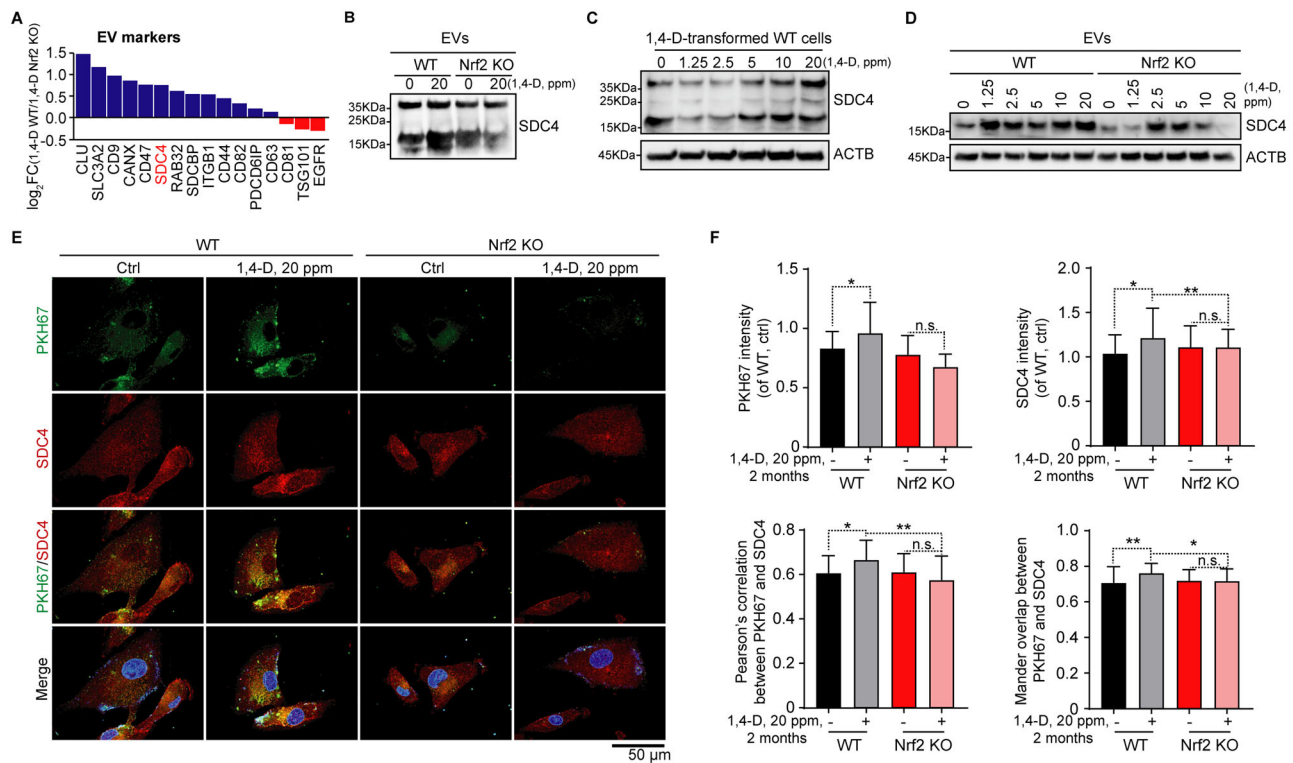
FIGURE 6 | 1,4-D-induced, SDC4-enriched EVs are significantly internalised by recipient cells. (A) Effects of Nrf2 knockout on the expression of key EV biomarkers based on EV proteomics. Data are shown as log2 fold changes. (B) Representative immunoblots showing the abundance of SDC4 in EVs derived from the indicated groups. (C) Representative immunoblots showing SDC4 abundance in WT cells transformed by 1,4-D at concentrations ranging from 1.25 to 20 ppm. (D) Representative immunoblots displaying SDC4 expression in EVs derived from WT and Nrf2 KO cells transformed by 1,4-D at concentrations ranging from 1.25 to 20 ppm. (E) Representative SDC4 staining of A549 cells after 24-h treatment with PKH67-labelled EVs derived from WT, 1,4-D-transformed WT, Nrf2 KO and 1,4-D-transformed Nrf2 KO cell groups. (F) Quantification results of PKH67 and SDC4 intensities, along with Pearson's correlation and Mander's overlap, are shown for the co-localisation between PKH67-labelled EVs and SDC4. Data are presented as mean ± SD, $n = 10$, *$p < 0.05$, **$p < 0.01$ vs. control (one-way ANOVA with Bonferroni's multiple comparisons test).

(TSS), exon 1 and the first intron (Figure 7A). Many of these peaks contained conserved antioxidant response element (ARE) with the core sequence TGAG/CTC, as previously reported (Bi et al. 2020). To determine whether these Nrf2 binding sites regulate SDC4 expression in response to 1,4-D, we performed ChIP-qPCR to assess Nrf2 occupancy at these ARE elements. As shown in Figure 7B, elements 1, 2, 4, 5 and 6 exhibited high levels of Nrf2 binding under basal conditions, with 1,4-D treatment having minimal impact on these sites. In contrast, element 3, despite containing a tentative ARE element (TGAT-GCAG), showed minimal Nrf2 binding under both basal and 1,4-D-treated conditions. Notably, elements 7 and 8 displayed moderate basal Nrf2 binding, which was significantly enhanced following 1,4-D treatment (1.27% in WT cells vs. 18.20% in 1,4-transformed WT cells), suggesting that these regions are critical regulatory elements mediating 1,4-D-induced, Nrf2-dependent SDC4 expression. To further elucidate SDC4's functional role in 1,4-D-induced EMT, we conducted *SDC4* knockdown and overexpression experiments in 1,4-D-transformed WT and Nrf2 KO cells, respectively (Figure 7C). We found that *SDC4* knockdown reduced the migration rate of 1,4-D-transformed WT cells, whereas *SDC4* overexpression enhanced the migration rate of 1,4-D-transformed Nrf2 KO cells (Figure 7D). Next, we examined SDC4 abundance in EVs isolated from 1,4-D-transformed WT and

Nrf2 KO cells following *SDC4* knockdown and overexpression, respectively. In the 1,4-D-transformed WT cells, *SDC4* siRNA treatment significantly reduced SDC4 levels in EVs (Figure 7E). Conversely, in 1,4-D-transformed Nrf2 KO cells, SDC4 abundance in EVs increased following *SDC4* overexpression (Figure 7E). As previously noted, three additional proteins—COL12A1, CAPG and NNMT—were identified as contributors to 1,4-D-induced EMT propagation, based on integrative analyses of cell and EV proteomics (Figure 5C,F). We assessed their expressions in EVs from 1,4-D-transformed WT and Nrf2 KO cells subjected to *SDC4* knockdown and overexpression, respectively. COL12A1, CAPG and NNMT exhibited expression trends similar to SDC4, suggesting potential co-regulation and functional interplay in modulating EMT propagation (Figure 7E). Also, these molecular changes correlated with a marked decrease in A549 cell proliferation, migration, and invasion following incubation with EVs from *SDC4*-knockdown 1,4-D-transformed WT cells, compared to the control group (Figure 7F–H). As expected, A549 cells treated with EVs from 1,4-D-transformed Nrf2 KO cells overexpressing SDC4 exhibited enhanced proliferation, migration, and invasion (Figure 7F–H). Taken together, these data strongly support the role of Nrf2 in regulating the SDC4 expression and the biogenesis of SDC4-enriched EVs, both of which are crucial in 1,4-D-induced EMT and carcinogenesis.
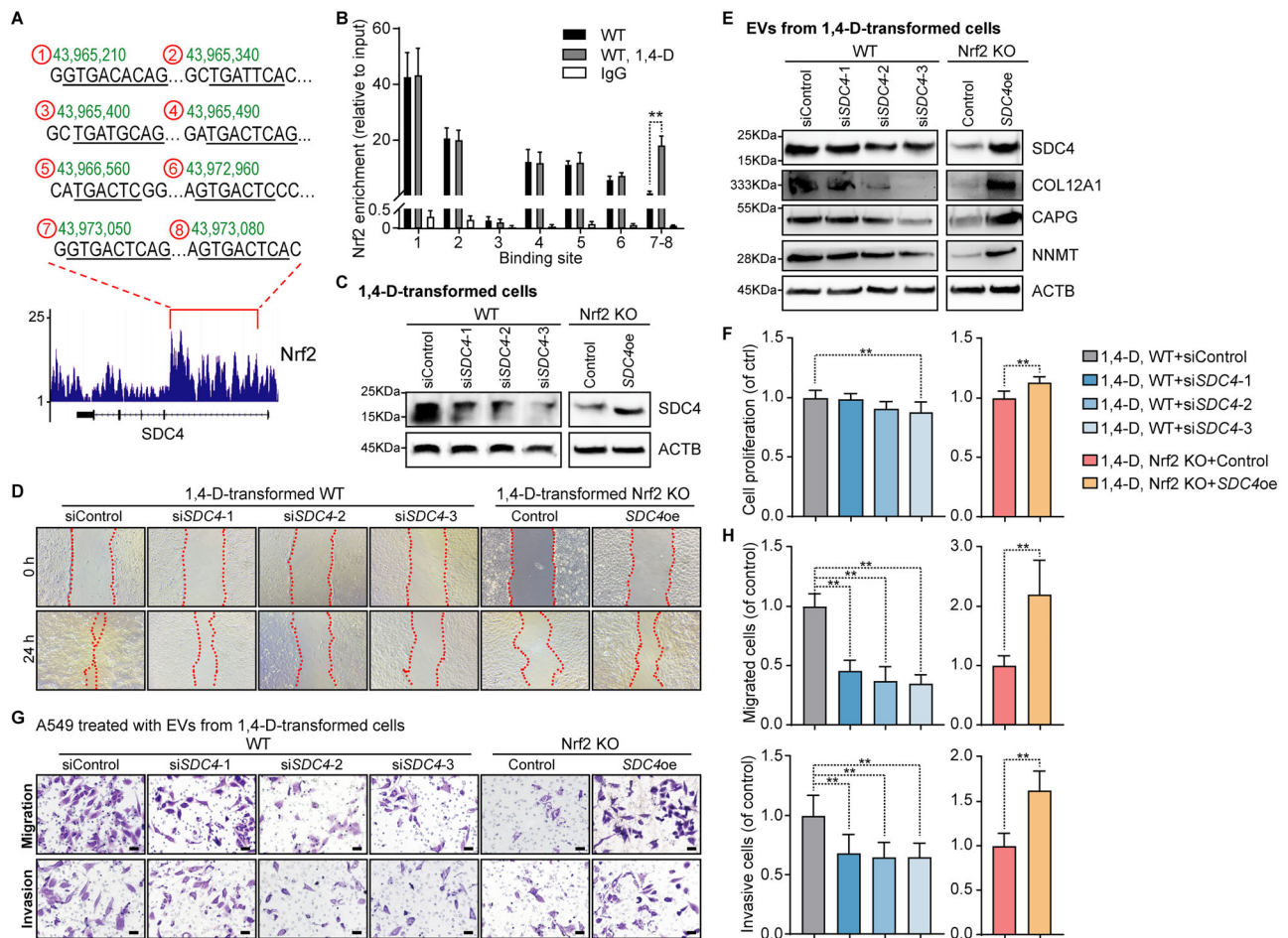
FIGURE 7 | Nrf2 modulates the 1,4-D-induced EMT process via SDC4 and SDC4-enriched EVs. (A) ChIP-seq analysis identifies Nrf2 binding peaks across the SDC4 gene body, with notable enrichment at the transcription start site (TSS), exon 1, and the first intron. Many of these peaks contain conserved antioxidant response element (ARE) featuring the core sequence TGAG/CTC. The predicted ARE sites on the SDC4 gene are marked with green numbers. (B) ChIP-qPCR analysis showing Nrf2 occupancy at these ARE elements on the SDC4 gene. Data are presented as mean ± SD, $n = 3$, **p < 0.01 vs. control (one-way ANOVA with Bonferroni's multiple comparisons test). (C) Representative immunoblots showing the abundance of SDC4 in 1,4-D-transformed WT cells with *SDC4* knockdown by siRNA and in 1,4-D-transformed Nrf2 KO cells with *SDC4* overexpression via the pcDNA3.1 vector. (D) Representative images from wound healing assay illustrating the effects of SDC4 regulation on the migration capabilities of 1,4-D-transformed WT and Nrf2 KO cells. (E) Representative immunoblots showing the abundance of SDC4, COL12A1, CAPG, NNMT and ACTB in EV samples derived from 1,4-D-transformed WT cells with *SDC4* knockdown and from 1,4-D-transformed Nrf2 KO cells with *SDC4* overexpression. (F) The effects of EVs derived from the indicated groups on A549 cell proliferation were determined by MTT assay. Data are presented as mean ± SD, $n = 6$, **p < 0.01 vs. control (one-way ANOVA with Bonferroni's multiple comparisons test or unpaired Student's t test). (G and H) Representative images illustrating changes in migration and invasion capabilities of A549 cells treated with EVs from the indicated groups, with quantification of migrated or invasive cells. Data are presented as mean ± SD, $n = 10$, **p < 0.01 vs. control (one-way ANOVA with Bonferroni's multiple comparisons test or unpaired Student's t test).

4 | Discussion

Accumulating evidence has highlighted the oncogenic properties of Nrf2 in cancer progression and metastasis (Rojo de la Vega et al. 2018). In this study, we demonstrated that 1,4-D consistently activates Nrf2 in a dose-dependent way, and this activation promotes the acquisition of EMT phenotypes in 1,4-D-treated cells. Notably, we unexpectedly discovered the connections between Nrf2 activation and the composition, release and function of EVs in cells subjected to long-term treatment of 1,4-D at environmentally relevant concentrations, a phenomenon that has not been previously recognised or reported. Upon cellular response to 1,4-D treatment, we observed Nrf2-dependent expression of gene *SDC4*, which governs the biogenesis, cargo selection and cell

tropism of EVs. Gain- or loss-of-function experiments for *SDC4* confirmed our hypothesis that Nrf2 modules *SDC4* expression and the release of SDC4-enriched EVs, thereby driving 1,4-D-induced EMT and potentially carcinogenesis. These findings not only suggest a role for Nrf2 in carcinogenesis but also reveal a previously unknown property of 1,4-D-induced Nrf2 activation in promoting EV biogenesis, a critical driver of carcinogenesis and cancer cell metastasis.

Earlier studies show the carcinogenicity of 1,4-D in the nasal cavity and liver (Stickney et al. 2003). Skin exposure of animals to 1,4-D has revealed its potential to cause cancer through the actions of other chemicals (Wilbur et al. 2012). In male A/J mice, a strain with a high spontaneous incidence of lung tumours,

intraperitoneal injection of 1,4-D increased the number of benign lung adenomas per animal (Maronpot et al. 1986). Recently, the US EPA evaluated the health risks of 1,4-D in occupational settings, highlighting concerns about its effects on the liver and nasal tissues (EPA 2024). However, the risks posed by 1,4-D in the general population through drinking water, inhalation or dermal contact have yet been fully assessed, leaving the associated health effects, beyond those on the liver and nasal tissues, unclear. Here, we provide direct evidence of the carcinogenic potential of 1,4-D at environmentally relevant concentrations in human bronchial epithelial cells. Moreover, our results from mouse xenograft experiments reveal liver metastasis associated with 1,4-D. These findings could prompt the International Agency for Research on Cancer (IARC) and the US EPA to reconsider the current classification of 1,4-D and provide a basis for more precise risk assessment and management of 1,4-D exposure in general population.

Nrf2 is a transcription factor primarily recognised for its role in regulating the expression of antioxidant and cytoprotective genes (Motohashi and Yamamoto 2004). Recent research has uncovered its complex, and context-dependent involvement in the EMT process and cell malignancy (Rojo de la Vega et al. 2018). Nrf2 activation promotes the expression of SNAIL (Chen et al. 2021), TWIST1 (Das et al. 2024) and ZEB1 (Wei et al. 2014), which drive the transition from epithelial to a mesenchymal phenotype. This transition is marked by decreased cell adhesion, increased motility, and enhanced invasiveness. Additionally, Nrf2 affects the remodelling of extracellular matrix (ECM), facilitating a microenvironment that supports EMT and enhances cancer cell aggressiveness (Muz et al. 2015). Moreover, Nrf2 plays a critical role in cancer progression by supporting the dissemination of cancer cells and the establishment of metastatic tumours (Shibata et al. 2010). Intriguingly, some studies have shown that Nrf2 knockout mice are more susceptible to chemically induced carcinogenesis (Iida et al. 2004; Wu et al. 2022), suggesting that Nrf2 might act as a tumour suppressor in certain contexts. Our pervious study indicated that Nrf2 mediates arsenic-induced generation of cancer-stem-like cells (CSCs) by activating HIF1α, a transcription factors that directly regulates the expression of a wide spectrum of genes critical for the acquisition of cellular stemness, such as *MYC*, *SOX2*, *KLF4*, *NAMPT*, *KIT*, *BACH1* and *ZEB1* (Bi et al. 2020). In this study, we observed that 1,4-D treatment not only upregulates stemness transcription factors like SOX2, MYC, FOXM1 and TBX5 but also increases the expression of genes associated with EV biogenesis, including SDC4 (Agere et al. 2018), TGFBI (Zhang et al. 2021) and FABP3 (Zhang et al. 2022), in an Nrf2-dependent manner. These findings further reinforce the oncogenic properties of Nrf2 and provide new insights into its role in promoting cancer metastasis through EV-mediated mechanisms.

Overwhelming evidence suggests the crucial role of EVs in cancer development and metastasis (Becker et al. 2016). EVs can transfer oncogenic signals from cancerous or chemically exposed cells to their neighbouring cells, promoting the spread of malignant traits and enhancing tumour progression (Raposo and Stoorvogel 2013). They also can alter immune cell function and modify the surrounding stroma and extracellular matrix, contributing to an immunosuppressive environment that allows tumour cells to evade immune surveillance (Benito-Martin et al. 2015; Sung

et al. 2015). Previous studies have suggested a link between EV cargoes and the Nrf2 pathway in oxidative stress-initiated cell or tissue damage (Vahidinia et al. 2024). However, the role of Nrf2-dependent EVs in cancer development and chemical carcinogenesis is still unclear. Our data indicates that Nrf2 activation facilitates the acquisition of EMT characteristics in 1,4-D-treated cells by directly increasing EMT protein expression and supplying EMT-promoting EVs. Interestingly, literature suggests that changes in EV concentration can mediate downstream effects. For example, Chen et al. (2023) demonstrated that steatotic hepatocyte-derived small extracellular vesicles (sEVs) promote foam cell formation and facilitate atherogenesis via the miR-30a-3p/ABCA1 axis, highlighting the functional consequences of altered EV secretion. In our study, we did not establish a direct connection between increased EV secretion and EMT propagation. However, we found that only the increase in EV numbers induced by 1,4-D under Nrf2 activation contributed to EMT propagation. This aligns with evidence that EVs carrying oncogenic or EMT-promoting cargo facilitate intercellular communication and tumour progression. Notably, Nrf2 knockout increased baseline EV numbers but significantly reduced EMT-related cargo compared to 1,4-D-treated WT cells. This finding underscores the importance of EV content over sheer quantity in determining their functional impact and highlights the need for deeper investigations into EV cargo in cancer research.

SDC4 is a heparan sulphate proteoglycan that interacts with the ECM and various growth factors (Elfenbein and Simons 2013). It is frequently overexpressed in cancers such as breast, prostate and colorectal cancers, where its overexpression is associated with poor prognosis and aggressive tumour behaviour (Győrffy 2024a, 2024b). Conversely, downregulation or loss of SDC4 expression also impacts cancer progression, depending on the specific cancer type and context. SDC4 is involved in several key signalling pathways, including those mediated by integrins and growth factor receptors like FGFR and PDGFR (Elfenbein and Simons 2013). Recent studies have elucidated the molecular mechanisms by which SDC4 contributes to cancer development, including its role in modulating tumour microenvironment and interacting with other cellular signalling components (Li et al. 2023). Given its role in tumour progression and metastasis, SDC4 is being investigated as a potential diagnostic and prognostic marker for neuroblastoma (Knelson et al. 2014). Its expression levels may offer valuable insights into tumour aggressiveness and help predict patient outcomes. In our study, we found that downregulation of SDC4 significantly inhibits the EMT properties of 1,4-D-transformed cells, reduces the release of SDC4-enriched EVs, and diminishes the EMT-promoting effects of 1,4-D-induced EVs. Remarkably, the effect of these EVs on cell proliferation was moderate in recipient cells, when compared to their effect on migration and invasion. To clarify this, we conducted a pathway enrichment analysis on proteins significantly upregulated by 1,4-D treatment in our EV proteomics (Figure S3). The analysis revealed that EMT was the most significantly induced. In contrast, cell proliferation-related pathways, such as MYC target v1 and MYC target v2, were inhibited by 1,4-D treatment. Since migration and invasion are key features of EMT, it is reasonable to expect that EVs from SDC4-enriched or silenced cells would have a stronger impact on these processes than on proliferation. These findings support the notion that EV-mediated signalling plays a crucial role in promoting EMT-related phenotypic changes, even in the

absence of significant effect on cell proliferation. Additionally, we unexpectedly observed liver metastasis in the 1,4-D-transformed WT cell group (Figure 2D). Based on the findings by Poças et al. (2023), which demonstrated that SDC4 regulates the motility of cancer cells and the liver tropism of cancer cell-derived EVs, we speculate that SDC4-enriched EVs contribute to liver metastasis by enhancing migratory and invasive phenotypes of 1,4-D-transformed cells and delivering EMT-promoting factors to the liver. Further investigations in *in vivo* models are necessary to substantiate this hypothesis.

Studies on EV cargo reveal intricate mechanisms through which EVs contribute to cancer progression, highlighting potential avenues for clinical intervention (Li et al. 2023). The function of EVs is influenced not only by their protein contents but also their lipids, nucleic acids and other components. Further studies are required to thoroughly analyse the molecular composition of EVs and explore the link between bioactive molecules in EVs and signal disruptions in recipient cells. Importantly, the present report elucidates the critical role of Nrf2 in mediating the expression and incorporation of SDC4 protein into EVs, thereby promoting malignant transformation induced by 1,4-D. These findings significantly advance our understanding of carcinogenesis and tumorigenesis associated with environmental exposure to 1,4-D.

5 | Conclusion

In conclusion, this study elucidated the oncogenic properties of Nrf2 in 1,4-D-induced transformation and carcinogenesis. Nrf2, consistently activated by 1,4-D, served as a key regulator of EMT protein expression within cells and their loading into EVs. It directly regulates the expression of SDC4, a surface protein involved in cancer development and metastasis, by binding to its first intron and activating transcription. As anticipated, Nrf2 deficiency mitigated the EMT phenotypes induced by 1,4-D by suppressing SDC4 expression and inhibiting the biogenesis of SDC4-enriched EVs, underscoring Nrf2's role as master regulator of SDC4. These findings provide valuable insights into the mechanisms underlying Nrf2 and EV's function in 1,4-D carcinogenesis. Further investigations are warranted to explore the specific cargo carried by SDC4-enriched EVs and the molecular alterations in the recipient cells, laying groundwork for developing therapeutic strategies against chemical carcinogenesis.

Author Contributions

Ziwei Wang: conceptualization (equal), data curation (equal), investigation (equal), methodology (equal), writing-original draft (equal). **Chitra Thakur**: investigation (equal), methodology (equal). **Zhuoyue Bi**: investigation (equal), methodology (equal). **Yiran Qiu**: investigation (equal), methodology (equal). **Wenxuan Zhang**: investigation (equal), methodology (equal). **Haoyan Ji**: investigation (equal), methodology (equal). **Arjun K. Venkatesan**: investigation(Equal), methodology(Equal). **Sashank Cherukuri**: data curation (equal), methodology (equal). **Ke Jian Liu**: data curation(Equal), methodology(Equal), **John D. Haley**: data curation(Equal), methodology(Equal). **Xinwei Mao**: data curation (equal), methodology (equal). **Jaymie Meliker**: data curation (equal), methodology (equal). **Fei Chen**: conceptualization (equal), funding acquisition (equal), project administration (equal), supervision (equal), writing-review and editing (equal).

Conflicts of Interest

The authors declare no conflicts of interest.

Data Availability Statement

All data included in this study are available upon request by contact with the corresponding author.

References

Agere, S. A., E. Y. Kim, N. Akhtar, and S. Ahmed. 2018. "Syndecans in Chronic Inflammatory and Autoimmune Diseases: Pathological Insights and Therapeutic Opportunities." *Journal of Cellular Physiology* 233, no. 9: 6346–6358.

Ashida, S., H. Nakagawa, T. Katagiri, et al. 2004. "Molecular Features of the Transition From Prostatic Intraepithelial Neoplasia (PIN) to Prostate Cancer: Genome-Wide Gene-Expression Profiles of Prostate Cancers and PINs." *Cancer Research* 64, no. 17: 5963–5972.

Becker, A., B. K. Thakur, J. M. Weiss, H. S. Kim, H. Peinado, and D. Lyden. 2016. "Extracellular Vesicles in Cancer: Cell-to-Cell Mediators of Metastasis." *Cancer Cell* 30, no. 6: 836–848.

Benito-Martin, A., A. Di Giannatale, S. Ceder, and H. Peinado. 2015. "The New Deal: A Potential Role for Secreted Vesicles in Innate Immunity and Tumor Progression." *Frontiers in Immunology* 6: 66.

Bi, Z., Q. Zhang, Y. Fu, et al. 2020. "Nrf2 and HIF1α Converge to Arsenic-Induced Metabolic Reprogramming and the Formation of the Cancer Stem-Like Cells." *Theranostics* 10, no. 9: 4134–4149.

Chen, X., S. Chen, J. Pang, et al. 2023. "Hepatic Steatosis Aggravates Atherosclerosis via Small Extracellular Vesicle-Mediated Inhibition of Cellular Cholesterol Efflux." *Journal of Hepatology* 79, no. 6: 1491–1501.

Chen, Y., X. Shao, J. Cao, et al. 2021. "Phosphorylation Regulates Cullin-Based Ubiquitination in Tumorigenesis." *Acta Pharmaceutica Sinica B* 11, no. 2: 309–321.

Chen, Y., Y. Wang, G. Charkoftaki, et al. 2022. "Oxidative Stress and Genotoxicity in 1,4-Dioxane Liver Toxicity as Evidenced in a Mouse Model of Glutathione Deficiency." *Science of the Total Environment* 806, no. pt. 2: 150703.

Chitti, S. V., S. Gummadi, T. Kang, et al. 2024. "Vesiclepedia 2024: An Extracellular Vesicles and Extracellular Particles Repository." *Nucleic Acids Research* 52, no. D1: D1694–1698.

Das, A., A. Mitra, S. Ghosh, et al. 2024. "Arsenic-Induced Transition of Thymic Inflammation-to-Fibrosis Involves Stat3-Twist1 Interaction: Melatonin to the Rescue." *Biofactors* 51, no. 1: e2110.

Dourson, M., J. Reichard, P. Nance, et al. 2014. "Mode of Action Analysis for Liver Tumors From Oral 1,4-Dioxane Exposures and Evidence-Based Dose Response Assessment." *Regulatory Toxicology and Pharmacology* 68, no. 3: 387–401.

Dourson, M. L., J. Higginbotham, J. Crum, et al. 2017. "Update: Mode of Action (MOA) for Liver Tumors Induced by Oral Exposure to 1,4-Dioxane." *Regulatory Toxicology and Pharmacology* 88: 45–55.

Elfenbein, A., and M. Simons. 2013. "Syndecan-4 Signaling at a Glance." *Journal of Cell Science* 126, no. pt. 17: 3799–3804.

EPA, U. S. 2023. Benchmark Dose Software (BMDS) (Build 3.3.2; Model Library Version 2023.03.1) [Computer Software]. https://www.epa.gov/bmds/download-bmds.

EPA, U. S. 2024. 2023 Draft Revised Risk Determination for 1,4-Dioxane.

Gao, L., H. J. Wang, C. Tian, and I. H. Zucker. 2021. "Skeletal Muscle Nrf2 Contributes to Exercise-Evoked Systemic Antioxidant Defense via Extracellular Vesicular Communication." *Exercise and Sport Sciences Reviews* 49, no. 3: 213–222.

Gi, M., M. Fujioka, A. Kakehashi, T. Okuno, et al. 2018. "In Vivo Positive Mutagenicity of 1,4-Dioxane and Quantitative Analysis of Its Mutagenicity and Carcinogenicity in Rats." *Archives of Toxicology* 92, no. 10: 3207–3221.

Ginsberg, G., Y. Chen, and V. Vasiliou. 2022. "Mechanistic Considerations in 1,4-Dioxane Cancer Risk Assessment." *Current Opinion in Environmental Science & Health* 30: 100407.

Godri Pollitt, K. J., J. H. Kim, J. Peccia, et al. 2019. "1,4-Dioxane as an Emerging Water Contaminant: State of the Science and Evaluation of Research Needs." *Science of the Total Environment* 690: 853–866.

Győrffy, B. 2024a. "Integrated Analysis of Public Datasets for the Discovery and Validation of Survival-Associated Genes in Solid Tumors." *Innovation (Camb)* 5, no. 3: 100625.

Győrffy, B. 2024b. "Transcriptome-Level Discovery of Survival-Associated Biomarkers and Therapy Targets in Non-Small-Cell Lung Cancer." *British Journal of Pharmacology* 181, no. 3: 362–374.

Hahn, M. E., A. R. Timme-Laragy, S. I. Karchner, and J. J. Stegeman. 2015. "Nrf2 and Nrf2-Related Proteins in Development and Developmental Toxicity: Insights From Studies in Zebrafish (*Danio rerio*)." *Free Radical Biology and Medicine* 88, no. pt B: 275–289.

Iida, K., K. Itoh, Y. Kumagai, et al. 2004. "Nrf2 is Essential for the Chemopreventive Efficacy of Oltipraz Against Urinary Bladder Carcinogenesis." *Cancer Research* 64, no. 18: 6424–6431.

Kalluri, R., and K. M. McAndrews. 2023. "The Role of Extracellular Vesicles in Cancer." *Cell* 186, no. 8: 1610–1626.

Kaplan, R. N., R. D. Riba, S. Zacharoulis, et al. 2005. "VEGFR1-Positive Haematopoietic Bone Marrow Progenitors Initiate the Pre-Metastatic Niche." *Nature* 438, no. 7069: 820–827.

Knelson, E. H., A. L. Gaviglio, J. C. Nee, et al. 2014. "Stromal Heparan Sulfate Differentiates Neuroblasts to Suppress Neuroblastoma Growth." *Journal of Clinical Investigation* 124, no. 7: 3016–3031.

Lafranconi, M., J. Anderson, R. Budinsky, et al. 2023. "An Integrated Assessment of the 1,4-Dioxane Cancer Mode of Action and Threshold Response in Rodents." *Regulatory Toxicology and Pharmacology* 142: 105428.

Larigot, L., L. Juricek, J. Dairou, and X. Coumoul. 2018. "AhR Signaling Pathways and Regulatory Functions." *Biochimie Open* 7: 1–9.

Li, C., Z. Zheng, X. Wu, et al. 2023. "Stiff Matrix Induced srGAP2 Tension Gradients Control Migration Direction in Triple-Negative Breast Cancer." *Theranostics* 13, no. 1: 59–76.

Lin, N., N. Ding, E. Meza-Wilson, et al. 2023. "Volatile Organic Compounds in Disposable Diapers and Baby Wipes in the US: A Survey of Products and Health Risks." *Environmental Science & Technology* 57, no. 37: 13732–13743.

Maronpot, R. R., M. B. Shimkin, H. P. Witschi, L. H. Smith, and J. M. Cline. 1986. "Strain a Mouse Pulmonary Tumor Test Results for Chemicals Previously Tested in the National Cancer Institute Carcinogenicity Tests." *JNCI: Journal of the National Cancer Institute* 76, no. 6: 1101–1112.

Motohashi, H., and M. Yamamoto. 2004. "Nrf2–Keap1 Defines a Physiologically Important Stress Response Mechanism." *Trends in Molecular Medicine* 10, no. 11: 549–557.

Muz, B., P. de la Puente, F. Azab, and A. K. Azab. 2015. "The Role of Hypoxia in Cancer Progression, Angiogenesis, Metastasis, and Resistance to Therapy." *Hypoxia (Auckland)* 3: 83–92.

Ni, H. M., B. L. Woolbright, J. Williams, et al. 2014. "Nrf2 Promotes the Development of Fibrosis and Tumorigenesis in Mice With Defective Hepatic Autophagy." *Journal of Hepatology* 61, no. 3: 617–625.

Poças, J., C. Marques, C. Gomes, et al. 2023. "Syndecan-4 Is a Maestro of Gastric Cancer Cell Invasion and Communication That Underscores Poor Survival." *PNAS* 120, no. 20: e2214853120.

Raposo, G., and W. Stoorvogel. 2013. "Extracellular Vesicles: Exosomes, Microvesicles, and Friends." *Journal of Cell Biology* 200, no. 4: 373–383.

Rojo de la Vega, M., E. Chapman, and D. D. Zhang. 2018. "NRF2 and the Hallmarks of Cancer." *Cancer Cell* 34, no. 1: 21–43.

Rosenblum, J. S., A. Liethen, and L. Miller-Robbie. 2024. "Prioritization and Risk Ranking of Regulated and Unregulated Chemicals in US Drinking Water." *Environmental Science & Technology* 58, no. 16: 6878–6889.

Shibata, T., S. Saito, A. Kokubu, T. Suzuki, M. Yamamoto, and S. Hirohashi. 2010. "Global Downstream Pathway Analysis Reveals a Dependence of Oncogenic NF-E2-Related Factor 2 Mutation on the mTOR Growth Signaling Pathway." *Cancer Research* 70, no. 22: 9095–9105.

Sporn, M. B., and K. T. Liby. 2012. "NRF2 and Cancer: The Good, the Bad and the Importance of Context." *Nature Reviews Cancer* 12, no. 8: 564–571.

Stickney, J. A., S. L. Sager, J. R. Clarkson, et al. 2003. "An Updated Evaluation of the Carcinogenic Potential of 1,4-Dioxane." *Regulatory Toxicology and Pharmacology: Rtp* 38, no. 2: 183–195.

Sung, B. H., T. Ketova, D. Hoshino, A. Zijlstra, and A. M. Weaver. 2015. "Directional Cell Movement Through Tissues Is Controlled by Exosome Secretion." *Nature Communications* 6: 7164.

Sweeney, L. M., K. D. Thrall, T. S. Poet, et al. 2008. "Physiologically Based Pharmacokinetic Modeling of 1,4-Dioxane in Rats, Mice, and Humans." *Toxicological Sciences* 101, no. 1: 32–50.

Tian, C., L. Gao, T. L. Rudebush, L. Yu, and I. H. Zucker. 2022. "Extracellular Vesicles Regulate Sympatho-Excitation by Nrf2 in Heart Failure." *Circulation Research* 131, no. 8: 687–700.

Tian, C., L. Gao, and I. H. Zucker. 2021. "Regulation of Nrf2 Signaling Pathway in Heart Failure: Role of Extracellular Vesicles and Non-Coding RNAs." *Free Radical Biology and Medicine* 167: 218–231.

Totsuka, Y., Y. Maesako, H. Ono, et al. 2020. "Comprehensive Analysis of DNA Adducts (DNA adductome analysis) in the Liver of Rats Treated With 1,4-Dioxane." *Proceedings of the Japan Academy Series B* 96, no. 5: 180–187.

Uysal-Onganer, P., Y. Kawano, M. Caro, et al. 2010. "Wnt-11 Promotes Neuroendocrine-Like Differentiation, Survival and Migration of Prostate Cancer Cells." *Molecular Cancer* 9: 55.

Vahidinia, Z., A. Azami Tameh, S. Barati, M. Izadpanah, and E. Seyed Hosseini. 2024. "Nrf2 activation: A Key Mechanism in Stem Cell Exosomes-Mediated Therapies." *Cellular & Molecular Biology Letters* 29, no. 1: 30.

Vuoriluoto, K., G. Högnäs, P. Meller, K. Lehti, and J. Ivaska. 2011. "Syndecan-1 and -4 Differentially Regulate Oncogenic K-ras Dependent Cell Invasion Into Collagen Through $\alpha2\beta1$ Integrin and MT1-MMP." *Matrix Biology* 30, no. 3: 207–217.

Wang, Y., G. Charkoftaki, E. Davidson, et al. 2022. "Oxidative Stress, Glutathione, and CYP2E1 in 1,4-Dioxane Liver Cytotoxicity and Genotoxicity: Insights From Animal Models." *Current Opinion in Environmental Science & Health* 29: 100389.

Wei, J., Y. Zhang, Y. Luo, et al. 2014. "Aldose Reductase Regulates miR-200a-3p/141-3p to Coordinate Keap1-Nrf2, Tgfβ1/2, and Zeb1/2 Signaling in Renal Mesangial Cells and the Renal Cortex of Diabetic Mice." *Free Radical Biology and Medicine* 67: 91–102.

Wilbur, S., D. Jones, J. F. Risher, et al. 2012. *Toxicological Profile for 1,4-Dioxane*. Agency for Toxic Substances and Disease Registry (US).

Wu, R., X. Chen, H. Wu, et al. 2022. "Nrf2 Activation Contributes to Hepatic Tumor-Augmenting Effects of Developmental Arsenic Exposure." *Science of the Total Environment* 837: 155685.

Wu, T., E. Hu, S. Xu, et al. 2021. "clusterProfiler 4.0: A Universal Enrichment Tool for Interpreting Omics Data." *Innovation (Camb)* 2, no. 3: 100141.

Xu, L., Y. Zhu, C. Li, et al. 2022. "Small Extracellular Vesicles Derived From Nrf2-Overexpressing Human Amniotic Mesenchymal Stem Cells Protect Against Lipopolysaccharide-Induced Acute Lung Injury by Inhibiting NLRP3." *Biology Direct* 17, no. 1: 35.

Zenker, M. J., R. C. Borden, and M. A. Barlaz. 2003. "Occurrence and Treatment of 1,4-Dioxane in Aqueous Environments." *Environmental Engineering Science* 20, no. 5: 423–432.

Zhang, Q., D. K. Jeppesen, J. N. Higginbotham, et al. 2021. "Supermeres Are Functional Extracellular Nanoparticles Replete With Disease Biomarkers and Therapeutic Targets." *Nature Cell Biology* 23, no. 12: 1240–1254.

Zhang, X., Y. Xu, L. Ma, et al. 2022. "Essential Roles of Exosome and circRNA_101093 on Ferroptosis Desensitization in Lung Adenocarcinoma." *Cancer Communications (Lond)* 42, no. 4: 287–313.

Supporting Information

Additional supporting information can be found online in the Supporting Information section.